Bioinspired and Biological Chitin and Chitosan Based Composites

-- Chemistry, Microstructure and Mineralization

Xiaolin Zhang

A dissertation
submitted in partial fulfillment of the
requirements for the degree of

Doctor of Philosophy
University of Washington
2017

Reading Committee:

Marco Rolandi, Chair

Dwayne Arola

Guozhong Cao

Program Authorized to Offer Degree:

Materials Science and Engineering

University of Washington

Abstract

Bioinspired and Biological Chitin and Chitosan Based Composites

-- Chemistry, Microstructure, and Mineralization

Xiaolin Zhang

Chair of the Supervisory Committee:
Affiliate Associate Professor Marco Rolandi
Department of Materials Science and Engineering

From the stiffness span of squid beaks to the toughness of seashells and the hardness of chiton teeth, natural biological materials have a broad range of exceptional mechanical properties. Tanning induced protein cross-linking dictates the transition from the stiff rostrum to the compliant wing of a squid beak. A highly ordered microstructural organization of chitin nanofiber network embedded within a protein matrix facilitates the toughness of seashells. Nano-crystalline magnetite minerals embedded within chitin nanofiber network gives the ultra hardness of chiton tooth. Inspired by these biological strategies for improved mechanical properties, my Ph.D. research has been focusing on engineering chitin and chitosan based composites with improved mechanical properties from chemistry, microstructure and mineralization. Projects include a squid beak mimics with stiffness span dictated by the degree of cross-linking, methods to control chitin-silk

molecular morphology including an electric-field assisted gelation method and a water vapor annealing method as well as a proof-of-concept chitin-GelMA hydrogel for tissue engineering applications, and using banana slug radula as a model to explore correlations from teeth morphology, chemical composition and mineralization, to mechanical behavior and functionalities.

TABLE OF CONTENTS

LIST OF FIGURES

ACKNOWLEDGEMENT

My Ph.D. work started at the University of Washington, and wrapped up at the University of California Santa Cruz due to our lab move. I would express my gratitude to everyone along this journey. Particularly, I would like to thank my Ph.D. advisor Professor Marco Rolandi, who offered me the opportunity to work in this exciting field of bioinspired materials, and gave me guidance and support in scientific research, as well as wisdoms in everyday life. I would like to thank all committee members, Professor Guozhong Cao, Professor Dwayne Arola, and Professor Francois Baneyx for their valuable inputs on my research work. I also would like to acknowledge the funding agency Office of the Naval Research (ONR) award #N000141410724 and #N000141612507 for the finanacial support that makes my research possible.

I am very grateful to my undergraduate advisor Professor Jennifer Lewis who gave me an opportunity to work in a most cutting-edge research environment since sophomore year, and Professor Jianjun Cheng who is a life-long mentor and offers valuable life advise until today.

I would also like to express my deepest appreciation to all my friends and colleagues during these years. Those countless nights of chats, laughter and tears help to make any sorrow to fade, and any difficulty to dissolve. I would like to thank A.E. for being such an amazing supportive friend, and her forever optimism. I would like to thank J.N., from whom I understand the meaning of passion and perseverance for life. I would like to thank X.S., the most aspiring and dedicated researcher I have ever encountered, who inspires me to think in a different perspective, and who walks me through the most stressful time in my the last six months of my graduate studies.

Last and most importantly, I would like to thank my parents, Shuhua Su and Zhixiong Zhang, for their continuous support. They love me all their life, and provide an environment suitable for my growing up with all their capabilities. They trust me, and give me the greatest degree of freedom to make every single decision, big or small, in my life. Transferring to the U.S. for undergraduate study and pursuing a Ph.D. degree in materials science are only two examples. Without their unconditional love and support, I would not become who I am today.

Chapter I: Introduction

1.1 Chitin and Chitosan

Chitin is the second most abundant natural polysaccharide after cellulose and is synthesized by a number of living organisms[1], from insect cuticles,[2, 3] exoskeletons of arthropods,[4] mollusk shells,[5] to cell walls of fungi and yeast[6]. Chitin is a co-polymer of *β-(*1-4)-linked *N*-acetyl-D-glucosamine and *D*-glucosamine units randomly or block-distributed throughout the main backbone (Fig. 1.1.1). The fully acetylated version of chitin is insoluble in most organic solvents due to the strong hydrogen bonding. As acetyl groups (x block) are replaced by amine groups (y block) in chitin, solubility increases with a more hydrophilic and positively charged polymer. The ratio percentage between acetyl and amine groups is defined as degree of acetylation (DA). When DA is greater than 50%, the polymer is typically referred to as chitin. On the other hand, the highly deacetylated derivative (DA<50%) of chitin, chitosan, is water processable, but does not self-assemble into nanofibers without extra processing.[1]

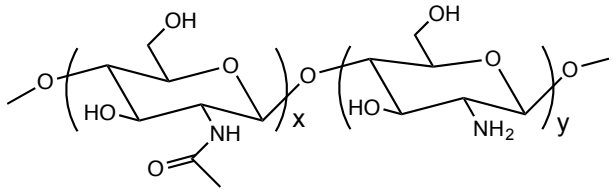

Figure 1.1.1 Chitin and chitosan chemical structure. Deacetylation replaces the N-acetyl-glucosamine group in chitin (x block) with an N-glucosamine (y block) resulting in a more hydrophilic and positively charged polymer. When the ratio between acetyl and amine groups is higher than 1:1 (x > y), the polymer is typically referred to as chitin.

Chitin exists in three different polymorphs in nature, α, β, and γ, which differ in molecular chain alignment and packing.[7] In most mineralized tissues such as the exoskeleton of crustaceans and cuticles of insects, chitin is in the α-form, where chitin chains are antiparallel aligned with intra-sheet hydrogen bonding. (Figure 1.1.2a) While in squid pens and some diatoms, it is in the β-form, where chitin chains are aligned in a parallel fashion. (Figure 1.1.2b) Moreover, in α-form, there exists some inter-sheet hydrogen bonding as well, which contributes to its stability.[8] The γ-form is recently reported as a variant of the α-form family.[9]

1.2 Cross-Linking Chemistry in Squid Beaks

The squid beak is an interesting example of a chitin-based material with unique properties. (Fig. 1.2.1) In contrast to mineralized composites, the squid beak is wholly

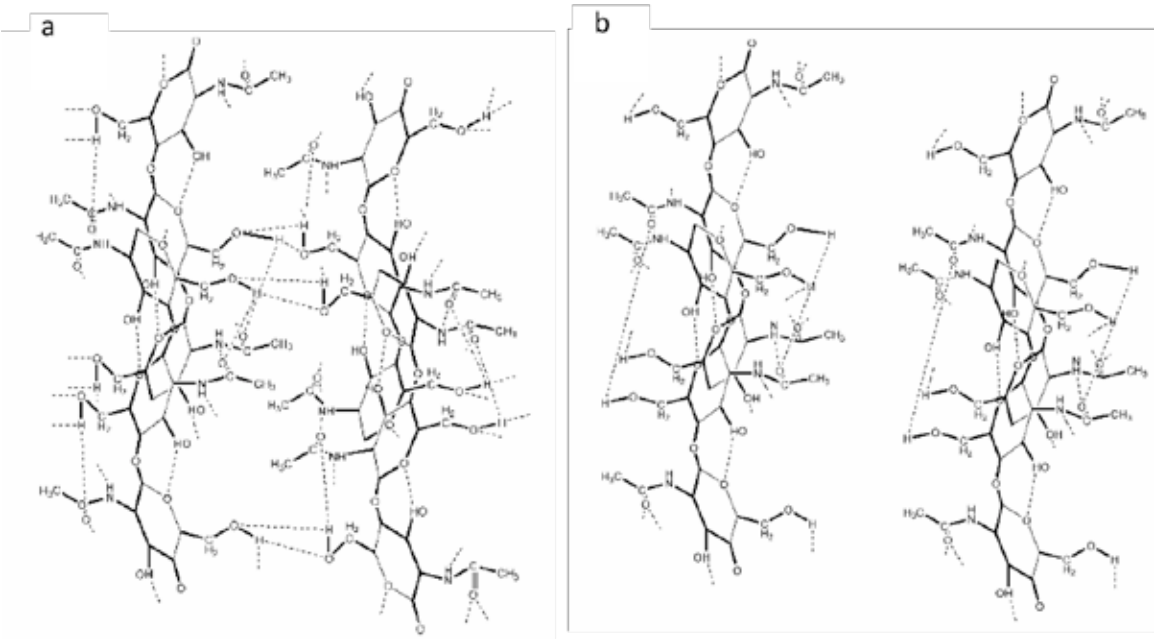

Figure 1.1.2 Molecular structure and hydrogen bonding in (a) alpha-chitin and (b) beta-chitin. Adapted from Ref. 6.

organic. The tip of the squid beak has a stiffness as high as 5 GPa without a mineralized phase and it couples this stiffness with a high fracture toughness of 3.2±1.5 MPa*$m^{1/2}$.[10, 11] A mechanical gradient is desired to bridge the mechanical mismatch from the rigid tip (5 GPa) to a soft compliant wing (50 MPa). [10, 11] This stiffness span from rigid to soft is a result of the tanning gradient. (Fig. 1.2.1b) Tanning is common in a number of invertebrates, such as mussel byssuses,[12] cockroach oothecae,[13] butterfly wings,[14] and most insect cuticles.[15] Tanning is the enzyme-catalyzed oxidation of compounds containing phenols. This oxidation creates cross-links that give the tanned material an increased stiffness with an associated darker color.[16, 17] The enzyme Tyrosinase catalyzes tanning with a cascade of chemical reactions that convert catecholamine compounds into compounds with increasing degrees of oxidation. In brief, L-3, 4-dihydroxyphenyl-alanine (L-dopa) turns into L-dopa quinone and L-dopa quinone oxidizes to benzoquinone. In turn, the primary amine on benzoquinone cyclizes into indole quinones.[18] The final oxidation product of tanning is often referred to as polydopamine[19]

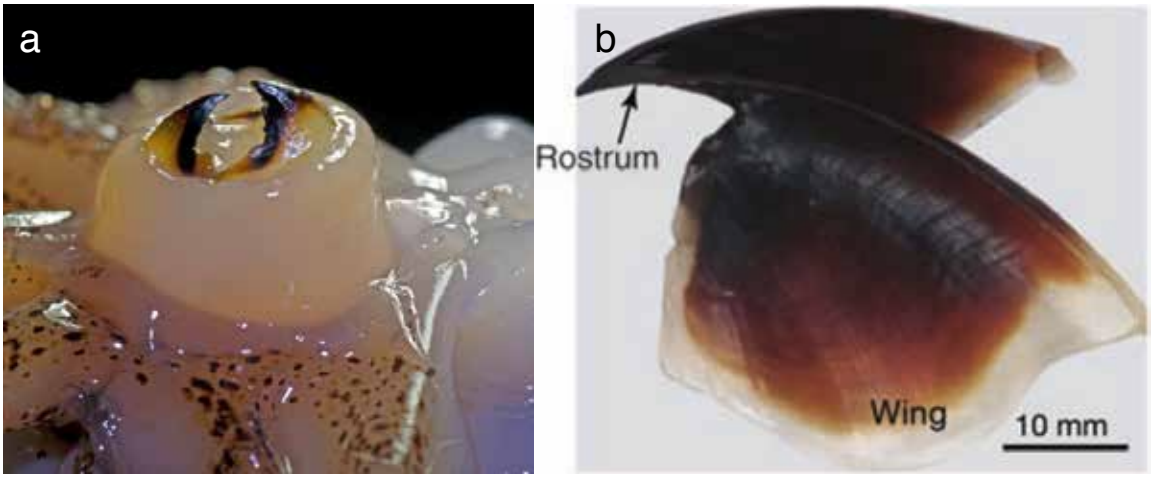

Figure 1.2.1 (a) Image of the beak of Humboldt squid *Dosidicus gigas*. (b) A close-up image of the upper beak, where the color goes from very dark at the rostrum to translucent at the wing edge.

or eumelanin.[20] The exact mechanism for this cascade of phenolic reactions in tanning is still under study.[19-21] It is, however, well understood that catecholamine-facilitated cross-linking contributes to the enhanced mechanical properties of all organisms with tanning gradients. [22, 23] The squid beak is one such example, where the tanning induced cross-linking dictates the mechanical span of the beak from the stiff rostrum to the compliant wing. For squid beaks, histidine, a major constituent of proteins in the beak, cross-links with L-dopa.[10] In addition to the cross-linking chemistry, an embedded chitin nanofiber network also contributes to the outstanding mechanical properties of the squid beak.[10]

1.3 Hierarchical Microstructure in Nature

Chitin molecules self-assemble into fibers, and organize into a hierarchical structure. (Fig. 1.3.1) 18-25 of such molecules assemble together and are wrapped with proteins to form nanofibrils that are 2-5nm in diameter, and about 300nm in length.[2, 3, 24] These nanofibrils cluster together and become fiber bundles roughly 50-300 nm in diameter. Successively the fiber bundles form into a sheet of branched networks. These sheets then stack up together with a twisted angle in between and become the ply-wood structure.[25] The complex hierarchical structure of chitin nanofibers at various structural levels leads to the remarkable mechanical properties of many natural biological materials. Nacre is one such example, where chitin nanofibers assemble within a protein matrix. This organic component is then mineralized with inorganic counterparts. The hierarchical organization of the mineralized chitin-protein fibers forming ply-wood structures impart the composites exceptional fracture toughness of 9MPa $m^{1/2}$.[26]

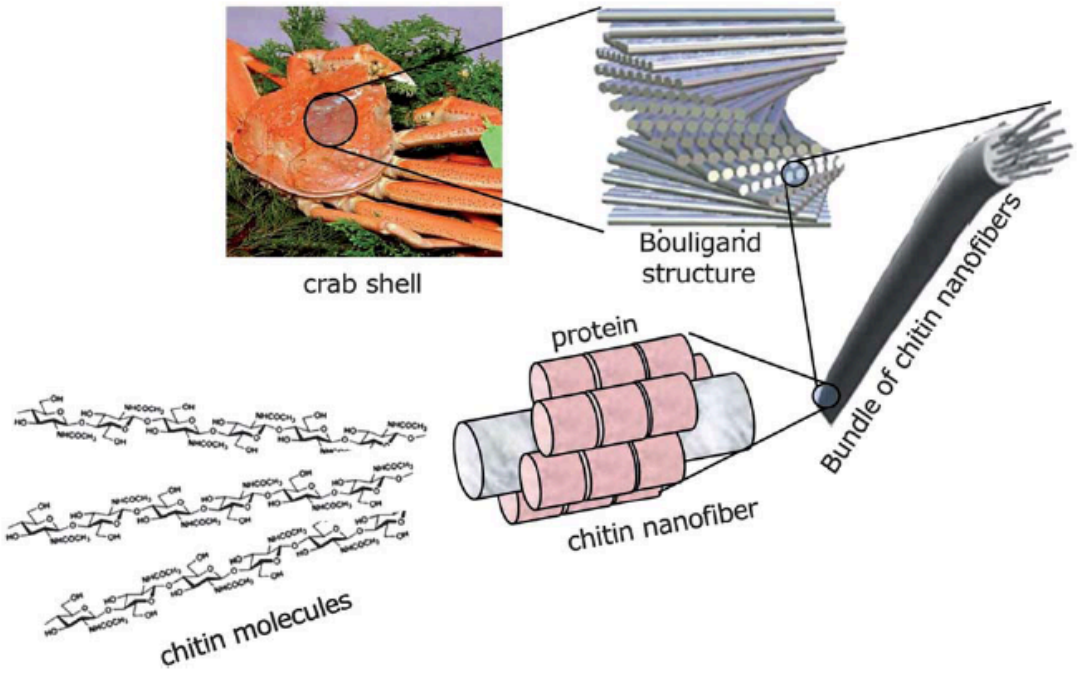

Figure 1.3.1 Hierarchical microstructure in a crustacean shell starting from individual chitin molecules. Adapted form Ref. 4.

Chitin nanofibers stand out for excellent thermal stability and sturdy mechanical properties while properly retaining their inherent biocompatibility, nontoxicity, physiological inertness, and biodegradability [27]. Due to these promising properties, scientist and engineers are designing materials to mimic such hierarchical organization. The main commercial sources of chitin are crab and shrimp shells, which are abundantly supplied as waste products from the seafood industry. Up to 100,000 million tons of chitin are disposed of yearly and only 10% of chitin's yearly production is utilized.[28] As such, chitin is an ideal candidate for structural biomaterial for drug release, tissue engineering, enzyme carriers, wound healing, biosensors, and medical implants.

1.4 Core-shell Mineralization in Chiton Tooth

Chiton is a marine mollusk that feeds on algae between rocks for food. The chiton tooth is known as the hardest material made by a living organism, (Fig. 1.4.1) with hardness as high as 7GPa. Teeth are arranged in parallel rows on a radula. Lowenstam first discovered in 1962, that the chiton tooth contains iron oxide in the magnetite structure.[29] Mature chiton teeth consist of a softer core capped by a hard magnetite layer. It was later revealed that during chiton tooth formation, chitin nanofibers form and bind with positively charged ions such as sodium and magnesium, whereas negatively charged proteins bind together with iron forming the magnetite structure.[30] The radula teeth work like a conveyor belt where a row of older teeth will be replaced by newer ones as they are

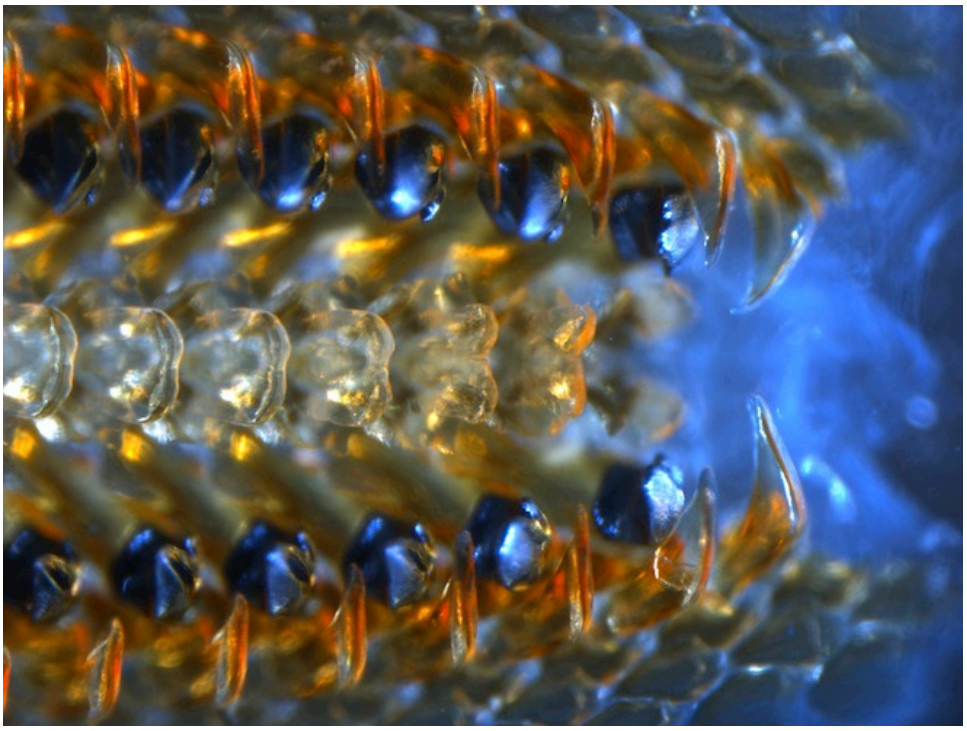

Figure 1.4.1 Reflected light optical micrograph of the tip of a *C. apiculata* radula, with four rows of fully mineralized teeth (arrow). Scale bar, 200 mm. Adapted from Ref. 30

worn out every few days.

A detailed study of the chiton tooth mineralization process has been carried out, dividing the structural and phase transformation into four distinct stages. First, a chitin nanofiber network gives the initial structure to the non-mineralized teeth. Then ferrihydrite crystals aggregate along the chitin nanofibers. Subsequently ferrihydrite crystal transforms into magnetite. And during the final stage, magnetite crystal continues to grow into parallel rods within the mature teeth. Such structural design and evolvement help the teeth to withstand abrasion, impact and fatigue when grazing rocks for food.

1.5 Chitin Nanofiber Synthesis

As we have discussed, chitin nanofibers are key structural components in many structural biological composites, and is a key promising material for the design of synthetic composite materials. However, chitin is challenging to work with due to its insolubility in most organic solvents and it is difficult to maintain the chitin nanofiber structure during processing.

There are in general two complementary routes to engineer biological material mimics, “top-down” and “bottom-up”. In the top-down approach, a natural material in bulk is regarded as one complex entity, and gets broken down to the individual building blocks of interest. In the “bottom-up” approach individual molecules are self-assembled to yield the desired product. Since chitin is difficult to fully dissolve to the molecular level, conventionally chitin nanofiber production largely relies on the “top-down” approach.

Crustacean shells are often used as the starting material. Pure chitin is isolated upon demineralization and deproteinization using acid and alkali treatments respectively.[31, 32] The purified chitin subsequently goes through acid hydrolysis in order to cleave the non-crystalline regions. The protonation of primary amine groups in acid environment leads to a more stable colloidal suspension with smaller nanofibers.[33, 34] A suspension with nanometer scale rods of chitin has been prepared from various sources such as crab shells,[33, 35-38] shrimp shells,[39, 40] and squid pens;[41] for α and β chitin respectively. Upon repetitive acid hydrolysis, the chitin suspension is dialyzed against water to neutral pH. Goodrich et al[39] demonstrated chitin nanofibers from blending the neutralized chitin suspension at high speed using a commercial blender and lyophilization. The resulting nanofibers from these protocols are typically 10-100 times larger than the biogenic counterpart (~ 3 nm) with large standard deviation in diameter. Smaller (10-20 nm) nanofibers are obtained by grinding the chitin suspension at neutral pH.[37] It is worth noting that, with this method, the starting material needs to be directly extracted from crustacean shells and kept in a hydrated state to avoid strong hydrogen bonding between the fiber bundles upon drying.[37, 40]

A modified version of this method is used to prepare chitin nanofibers from mushrooms, with an additional de-coloration step and an alkali treatment, to yield nanofibers that are 20-28 nm in diameter.[42] This method also requires the starting material to be in the hydrated state. Ifuku et al. reported that nanofibers from dry chitin are obtained with mechanical treatment under acidic condition (Fig. 1.5.1).[38] In brief, dry chitin (Fig. 1.5.1a) is dispersed at pH 3. At pH 3, the primary amines on chitin are protonated and

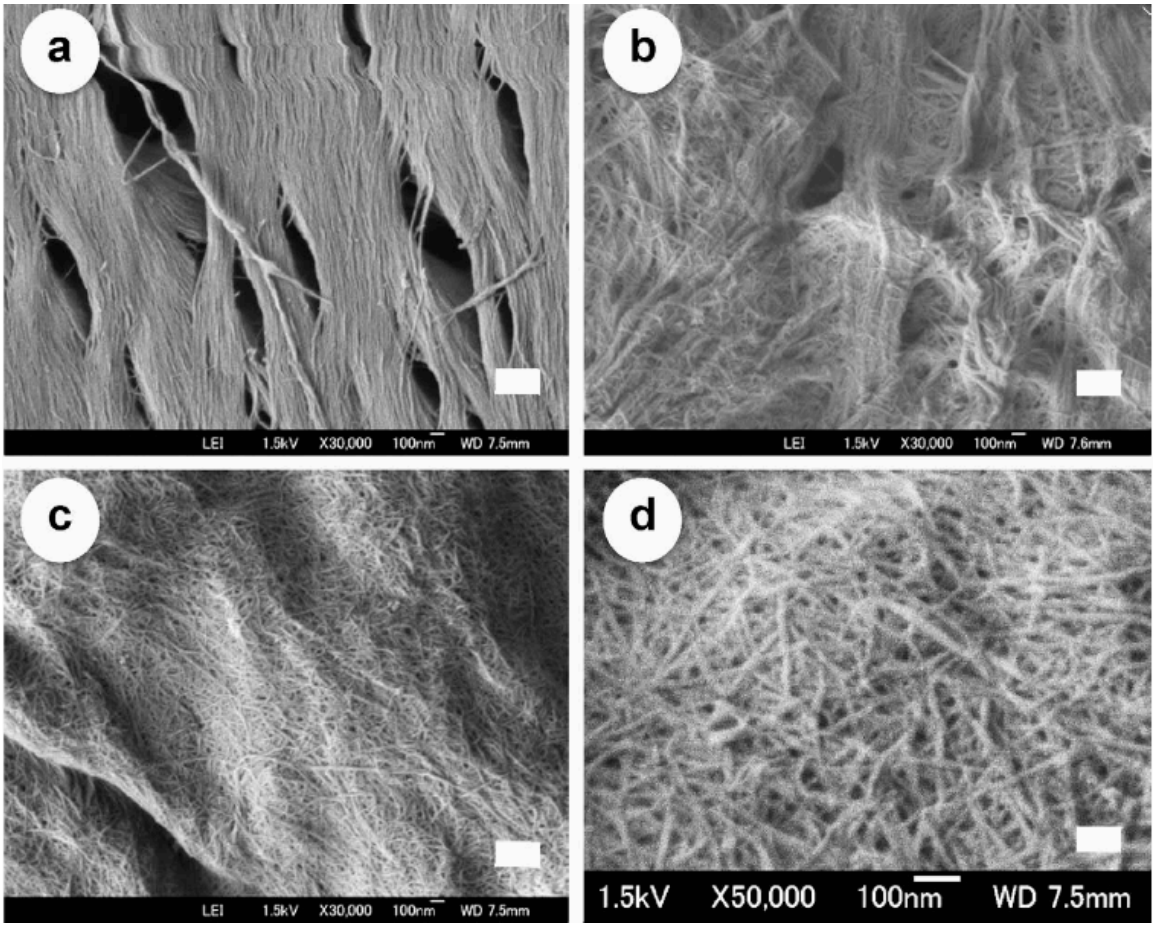

Figure 1.5.1 FE-SEM micrographs of (a) crab shell after removing matrix components, and chitin fibers after one pass through the grinder treated (b) without and (c and d) with acetic acid. The length of the scale bar is (a–c) 300 nm, and (d) 100 nm respectively. Reproduced from Ref. 38 with permission from Elsevier.

the charge present on the chitin facilitates dissolution and nanofiber formation upon crushing and grinding. In contrast, the same treatment at neutral pH yields thick fiber bundles (Fig. 1.5.1b). At pH 3, fine chitin nanofibers are observed with a width of 10-20 nm and high aspect ratios (Fig. 1.5.1 c, d).

Chitin nanofibers can also be prepared in milder conditions using high-pressure homogenization. A dispersion of pristine chitin at pH 4.1 is processed through a high-pressure homogenizer with 0.2 mm nozzle at a pressure of 15,000 psi for 20 passes

followed by 0.13 mm nozzle at 22,000 psi for 10 passes[43]. The final chitin/water dispersion is then casted into a thin film with an average nanofiber diameter of 20nm. (Fig. 1.5.2)

Another "top-down" top down approach to prepare chitin nanofibers is mediated oxidation with strong acid hydrolysis (e.g. 3M HCl at 90°C for 1.5hr), intensive mechanical disintegration, and 2,2,6,6-tetramethylpiperidine-1-oxyl radical (TEMPO). First, chitin is solubilized in water by selective oxidation of the primary hydroxyl groups

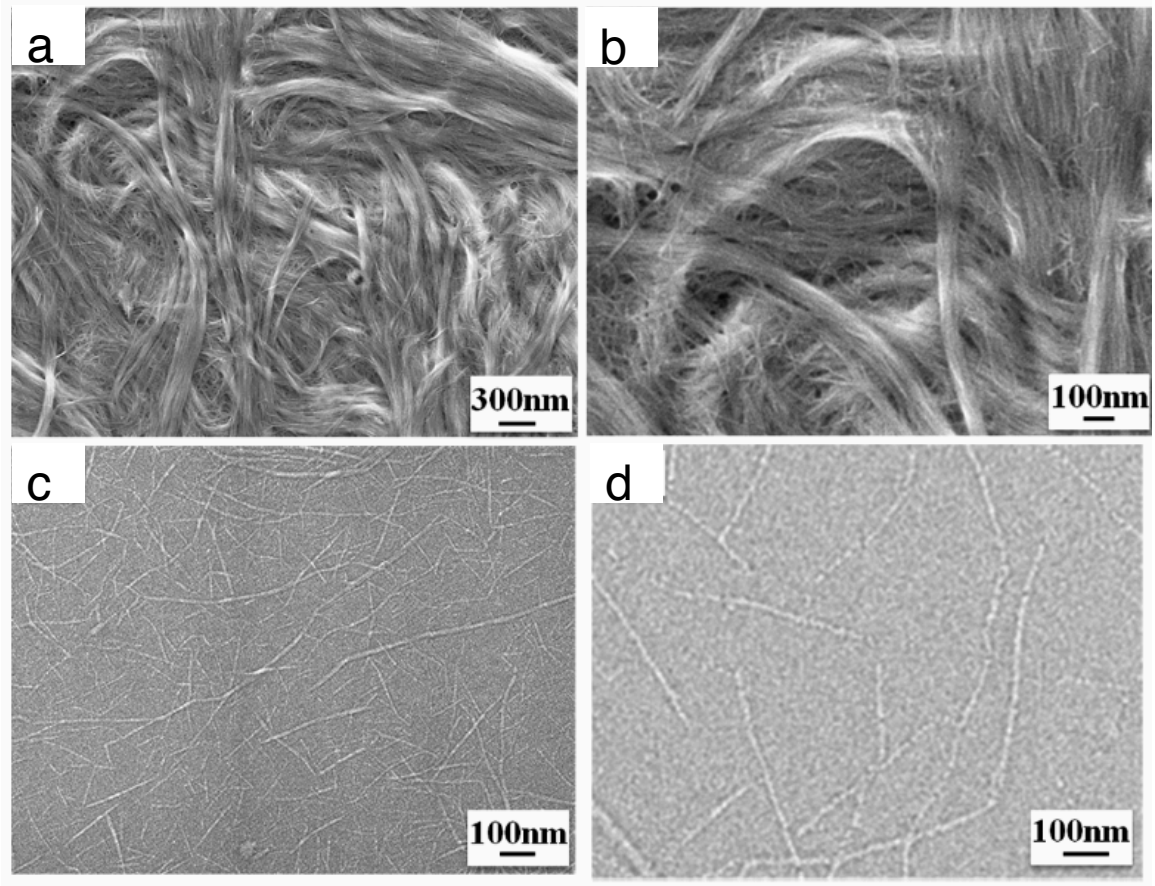

Figure 1.5.2 (a, b) SEM images of the cationized chitin and homogenized chitin with a pH of 4.1, respectively; (c, d) SEM images with higher magnification in comparison to (a) and (b), respectively. Reproduced from Ref. 43 with permission from the ACS Publications.

with the aid of sodium hypochlorite (NaClO) as a co-oxidant.[44, 45] The primary hydroxyl groups are selectively oxidized to carboxylate groups. By optimizing the concentration of NaClO added to the system, the water-insoluble content can be tuned, while keeping the degree of N-acetylation mostly unchanged.[46] (Fig. 1.5.3) An increased amount of NaClO in the system leads to prolonged oxidation time, and a decrease in the weight percentage of water-insoluble fraction, without achieving complete dissolution. (Fig. 1.5.3a) The carboxylate content and the amount of NaClO added are linearly correlated while the degree of N-acetylation of the water-insoluble fractions remains almost constant (Fig. 1.5.3b) The resulting carboxylate groups are negatively charged on the surface of chitin crystallites and promote dissolution into chitin nanofibers. The resulting water-insoluble fraction is obtained by centrifuge with excessive washing with water, and re-dispersed in water with ultrasonic treatment. Different NaClO concentrations result in fiber slight different fiber morphology, with an average of 8nm in width (Fig. 1.5.3c).

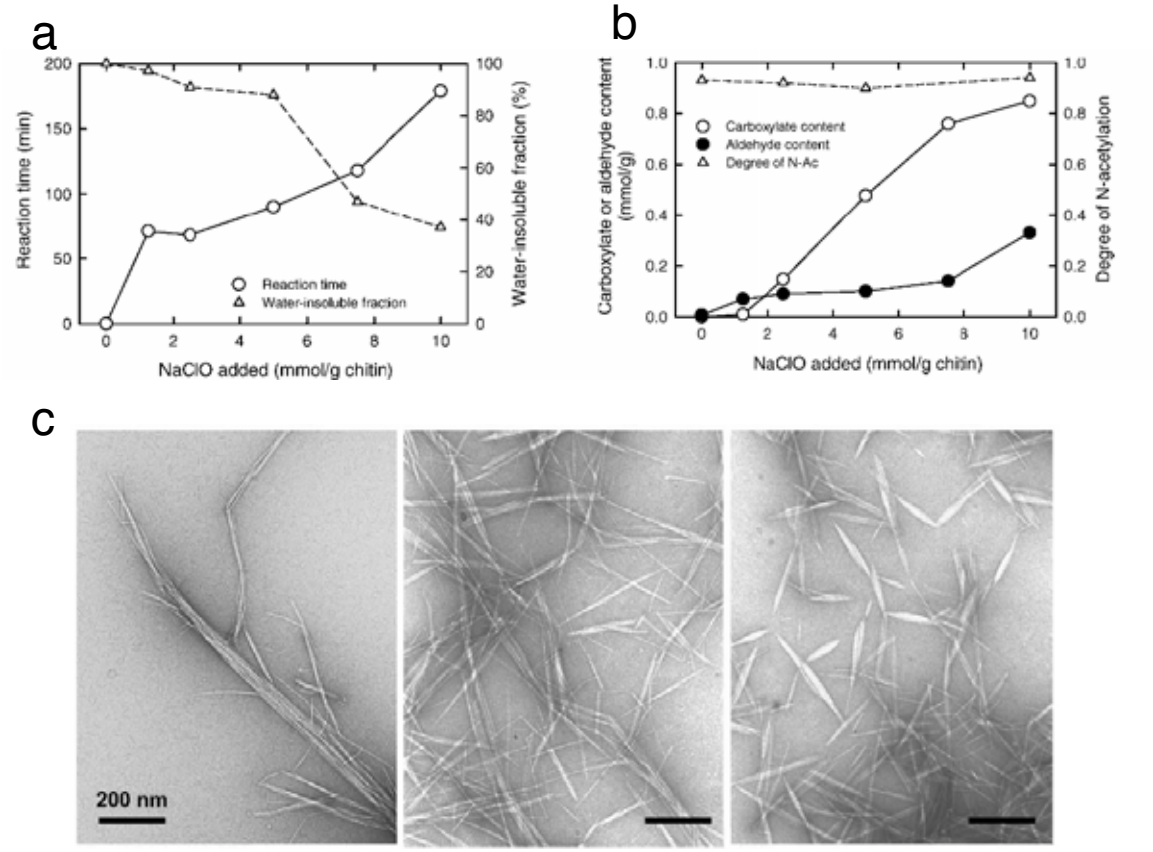

Figure 1.5.3 (a) Relationships between the amount of NaClO added in the TEMPO-mediated oxidation of chitin and either the total reaction time or the weight ratio of the water-insoluble fraction. (b) Relationships between the amount of NaClO added in the TEMPO-mediated oxidation of chitin and either the carboxylate or aldehyde content of the water-insoluble fraction. The degree of N-acetylation is also plotted.(c) Transmission electron micrographs of TEMPO-oxidized chitin nanocrystals prepared under different conditions. Adapted from Ref. 46 with permission from the ACS Publications.

A similar route to separate chitin into individual nanofibers is to use the electrostatic repulsion that occurs during partial deacetylation of chitin into chitosan and subsequent protonation of the resulting primary amines.[47] To this end, a pristine chitin powder from crab shells is treated with 33% NaOH at elevated temperature to increase the degree of deacetylation and the number of primary amines. Protonated primary amines increase the charge on the chitin crystallite and result in increased electrostatic repulsion between the

chitin molecules. Mechanical disintegration yields individual chitin nanofibers of *ca*. 6 nm in diameter and a higher aspect ratio than the TEMPO-mediated ones.[48] These chitin nanofibers produced from either TEMPO-mediated oxidation or partial deacetylation can be further casted into thin films.

Oh et al recently developed a chemical-etching free approach to disintegrate chitin using calcium ions and via solvent exchange.[49] This approach results into a chiral nematic phase with a hierarchical nature that mimics the Bouligand structure found in nature (Fig.1.5.4). In brief, a chitin gel is prepared by dissolving chitin in Ca-saturated methanol solution.[50] Ca^{2+} ions bind to the hydroxyl groups in the chitin and disrupt intramolecular hydrogen bonding. Upon chitin physical dispersion, Ca^{2+} ions are removed through solvent exchange using methanol, isopropanol (IPA), and deionized water (Fig. 1.5.4a). This process yields chitin nanofibers are in either the nematic or liquid crystalline phase in alcohol (Fig.1.5.4b, c), or in chiral nematic phase as a hydrogel (Fig. 1.5.4d).

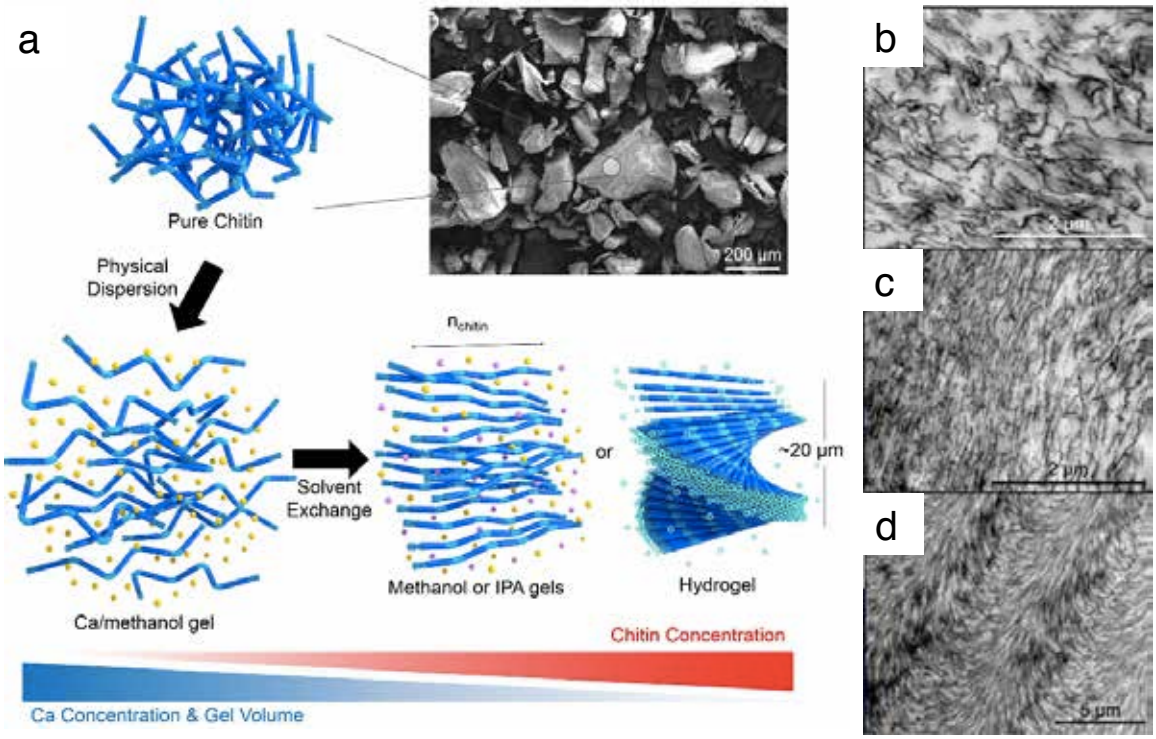

Figure 1.5.4 (a) Calcium-saturated methanol disintegrates chitin nanofbrils with minimal chemical modification, generating a Ca-methanol gel (disordered) (bottom-left panel). Ca2+ are removed from the Ca-methanol gel by washing with alcohol (methanol or IPA) and DI water, thus generating alcohol gels (methanol gel or IPA gel) in the N phase (bottom-middle panel) and a hydrogel in the N* phase (bottom-right panel). The yellow, pink, and blue beads represent three different types of solvent molecules: methanol-solvated Ca2+, alcohol (methanol or IPA), and water. (b) TEM images showing morphological change of chitin nanowires by solvent exchange of Ca-methanol gel (b), IPA gel (c), and hydrogel. Reproduced from Ref. 49 under a Creative Commons CC-BY license.

Bottom-up In contrast to "top-down", in the bottom-up approach building blocks of interest are assembled from individual molecules into highly organized structures. The bottom-up approach requires chitin molecules to be dissolved before assembling into chitin nanofibers. Due to chitin general insolubility in water and most organic solvents, this approach is limited to few solvent systems.[51]

Electrospinning of depolymerized chitin solution is a technique that is widely used for nanofiber assembly. [52, 53] In electrospinning, a high voltage is applied to a metallic capillary, which is connected to the solution reservoir. With a sufficient high electric field, electrostatic forces then overcome the surface tension in the solution, which forms a polymer jet from the capillary nozzle. This jet solidifies in nanofibers upon hitting a substrate of choice. To create an electrospinning solution, chitin is first depolymerized via gamma radiation to improve its solubility and then dissolved in 1,1,1,3,3,3-

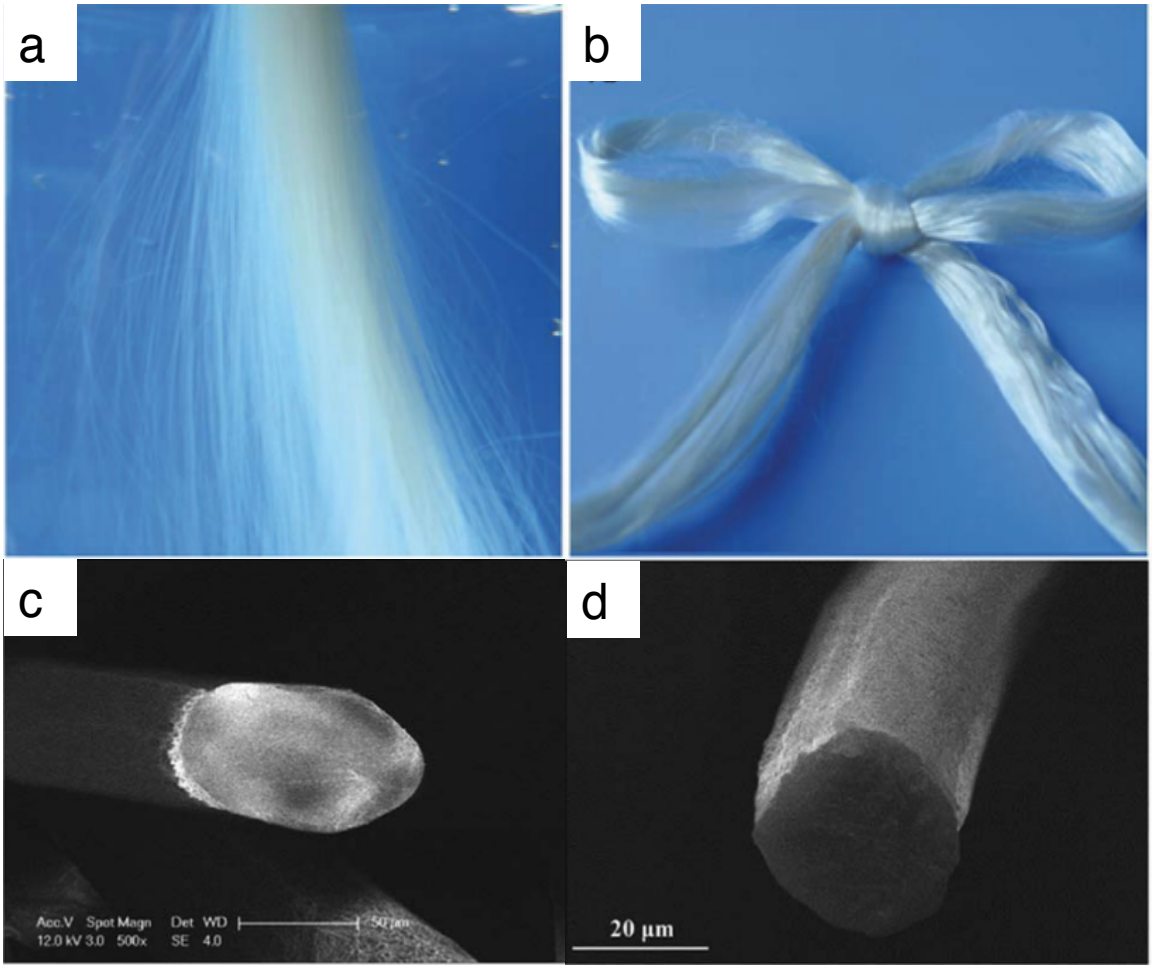

Figure 1.5.5 Photograph of (a) freshly spun chitin fibers in water and (b) air-dried fibers. SEM images of the chitin fibers (a) lyophilized and fractured in liquid nitrogen and (b) air-dried. Reproduced from Ref. 59 with permission from the Royal Society of Chemistry.

hexafluoro-2-propanol (HFIP). The electrospun nanofibers have an average diameter of 160 nm with a broad range from 50-460 nm.

Alternatively, ionic liquids are used to dissolve chitin and create an electrospinning solution.[54-56] Examples include 1-butyl-3-methyl-imidazolium chloride ([C_4mim]Cl) used at 110°C[54] and 1-allyl-3-methyl-imidazolium bromide ([Amim]Br).[55] Using the dry-jet-wet-spinning method,[57] chitin is dissolved in an acetate salt solution and spun into microscale fibers.[58] Zhang et al reported that pure chitin microfibers are spun directly from chitin dissolved in NaOH-urea upon several freeze-thawing cycles.[59] These microfibers have an average diameter between 30 μm and 80 μm. (Fig.1.5.5)

Rolandi group has developed methods to self-assemble chitin nanofibers from solutions of chitin in organic solvents without requiring electro-spinning (Fig.1.5.6).[47, 60, 61] Appropriate amounts of chitin starting material (β-chitin from squid pen) are dissolved in HFIP or LiCl/N,Ndimethylacetamide (DMAC), which causes hydrogen bond disruption. These solvents only work with β-chitin as the striating material because β-chitin has a lower degree of hydrogen bonding than α-chitin. The self-assembly process is then initiated via solvent evaporation of HFIP or precipitation by addition of water for LiCl/DMAC. For LiCl/DMAC, small (*ca.* 3nm) and intermediate (*ca.* 6nm) sizes of fibers adhere to the larger fiber bundles (*ca.* 10nm). In comparison, HFIP- chitin solutions form monodispersed chitin nanofiber of 3 nm in diameter (Fig. 1.5.6 a-c). Interestingly, these nanofibers are α-chitin, which is the more energetically favorable crystalline structure of chitin. These 3 nm self-assembled α-chitin remarkably match the nanofibers found in crustaceans shells and arthropod cuticles in dimensions and

crystalline structure, and are versatile building blocks for engineering biomimetic chitin nanofiber assemblies.

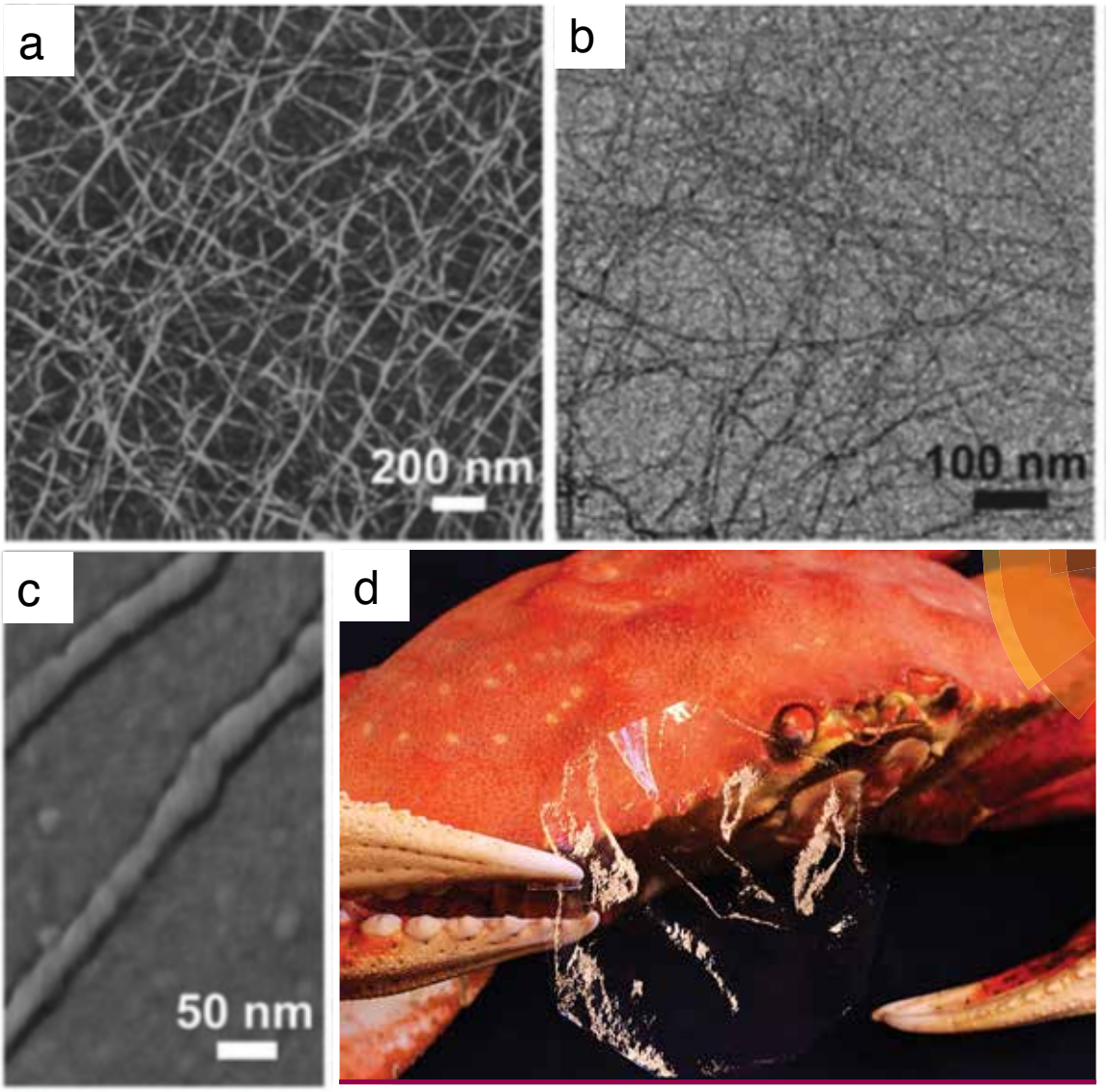

Figure 1.5.6 The morphology and diameter distribution of chitin nanofibers. In the AFM images, the apparent nanofiber width is larger due to tip convolution. (a–c) 3 nm nanofibers prepared from HFIP solution (5 mL, 0.01 wt%): (a) AFM height image, (b) bright field TEM image, (c) AFM phase image of two fibers. (d) thin transparent chitin film fabricated from HFIP solution drop-casting. Reproduced from Ref. 60 (a-c) and Ref. 61 (d) with permission from the Royal Society of Chemistry.

1.6 Chitosan Processing, Properties and Applications

As it is briefly introduced in section 1.1, chitosan is the highly deacetylated form of chitin, which does not self-assemble into nanofibers due to a lack of acetyl groups and hydrogen bonding. Instead, the presence of amino groups improves water solubility of chitosan. The solubility comes from the protonation of $-NH_2$ group on the C-2 position of the D-glucosamine unit.[62] Thanks to the solubility capability of chitosan in aqueous solution, chitosan is widely used in a large number of applications in the form of hydrogels, fibers, thin films and sponges.

Hydrogels are prepared from hydrophilic polymers, of which functional groups allows the binding between polymer chains and become stable with high water content. Chitosan based hydrogel networks can be prepared from either physical association or chemical bonding.[63-65] There are four major physical association mechanism, which are ionic, polyelectrolyte, polymer complex and hydrophobic interactions.[64] All of these could lead to chitosan gelation, however, a pure physical chitosan gel can be reversed. To better stabilize chitosan hydrogel, chemical cross-linking is an alternative to produce robust hydrogel network. Such cross-linking can be achieved with either small molecule cross-linkers such as glutaraldehyde, diisocyanate, and diglycidyl ether.[63] Photo-crosslinking can also be achieved by modifying chitosan molecule with photo-sensitive functionalities, such as azides or acrylates.[65] These covalently reinforced chitosan hydrogel becomes very stable while retaining high water content.

Electrospinning is a widely used method to create fiber morphology. Chitosan dissolved in diluted acids such as acetic acids can be electrospun into fibers, as the experimental set-up explained in Section1.3. Many attempts have been made to produce chitosan fibers. In a conventional wet-spinning process, chitosan dissolved in dilute acid solutions are extruded through a spinneret that is immersed in a coagulation bath. Viscous chitosan solutions is transformed into fibers in different coagulation baths such as solutions of NaOH,[66] KOH,[67] calcium chloride or acetate,[68] etc. Smooth and uniform striated fibrous surface could be obtained by using a highly deacetylated chitosan (DA=2.7%) The coagulated fibers can be washed in water to remove excess coagulant, dried and collected. To simplify the processing and to control the swelling behavior better, a pseudo-dry-pinning process is developed which instead of solution bath, a gaseous ammonia is used to neutralize and stabilize the as-spun chitosan fibers.[69] Due to the amino group protonation from dilute acid solutions, a dry-spinning process of pure chitosan has never been reported due to its instability. Reacetylation is one route, which the acetylated chitosan fibers show good thermal stability and improved mechanical strength.[67] Other modifications have also be attempted, such as co-spinning of poly(lactide-co-glycolide) (PLGA) and chitosan/poly(vinyl alcohol) for enhanced elastic modulus and strength along with degradation period.[70] In addition to chitosan hydrogels and electro-spun fibers, chitosan can also be prepared in other forms such as thin films or sponges. Drop casting or spin coating can produce chitosan thin films. Sponges are typically produced by freeze-drying method.

Chitosan, besides its versatile processability, it is also non-toxic, biocompatible, biodegradable, and can be sterilized. These properties make chitosan a good candidate for a wide range of applications in biomedical and biological fields.[62] Pristine chitosan hydrogel is not entirely stable, which at the same time, serves as the carrier for gene or drug carrier for cancer therapy and drug delivery purposes. Depending on the delivery system requirements, a prolonged delivery can be achieved with chemical modification of chitosan hydrogel, as well as control of drug loading by local entrapment or covalent bonding.[64] Electro-spun chitosan substrates have gained lots of traction in tissue engineering and regenerative medicine field due to their fibrous porous structure. The porous structure, as compared to bulk gel, allows a more effective oxygen and nutrient transport. Meanwhile the fibrous structure mimics the extracellular morphologies for cardiomyocytes or neuron cells, which improves cell elongation and alignment. Nevertheless the antimicrobial properties make chitosan substrates an attractive material for wound healing and wound dressing.[6]

1.7 Research Objective

The objective of my Ph.D. research is to mimic biological strategies for improving mechanical properties of materials by engineering and optimizing chitin based composites. With a systematic understanding of some biological examples, I tackle this problem from three aspects, chemistry, microstructure and mineralization. First in Chapter II, my work is focused on creating highly deacetylated chitin composites as a squid beak mimic. By tuning the crosslinking density of amine groups using catecholamine as a cross-linker, the stiffness and strength of chitosan can be doubled

compared to un-crosslinked chitosan. Then in Chapter III, I will focus on chitin nanofiber self-assembly in a protein matrix with enhanced control of the molecular morphology. I will start with understanding of chitin-silk molecular co-assembly by visualizing the localized elastic modulus mapping of chitin-silk composite with the aid of Atomic Force Microscope (AFM). Then I will introduce my work on electric field assisted chitin-silk gelation (e-gel) to control the molecular morphology, which, as a result, the ductility of chitin is largely increased. To tune the composite microstructure, I also investigate the mechanical response of water vapor annealed chitin-silk composites. Nevertheless, I will demonstrate a proof-of-concept hydrogel substrate by chitin nanofiber self-assembly within gelatin methacrylate (GelMA) hydrogel. In Chapter IV, I start to explore the tooth of banana slug radula, of which, the major component is beta-chitin, and to explore the correlations from teeth morphology, chemical composition and mineralization, to mechanical behavior and functionalities. This finding will serve as a first-of-its-kind detailed characterization of terrestrial mollusk radula teeth, and provide design cues for mineralized biomimetics with enhanced mechanical performance. Finally in Chapter V, I will summarize my findings and express my understanding in this field by providing some remaining challenges that needs to be tackled.

Chapter II: Squid Beak Chemistry Inspired Chitosan Composites

2.1 Background

Squid Beak Chemistry As a wholly organic material, the tip of the squid beak has a stiffness as high as 5 GPa without a mineralized phase and it couples this stiffness with a high fracture toughness of 3.2±1.5 MPa*m$^{1/2}$.[10, 11] Such a hard and rigid material would damage the soft squid tissue itself. In order to overcome this challenge, the squid beak spans two orders of magnitude in stiffness with a very rigid tip (5 GPa) to a soft compliant wing (50 MPa) that connects the beak to the squid mouth.[10, 11] This gradient in stiffness is a result of a gradual decrease in tanning from the tip to the wing (Fig. 1.4.1 b). As introduced in Section 1.4, catecholamine-facilitated cross-linking contributes to the stiffness span with tanning gradients.[71] The squid beak is made of histidine rich proteins with chitin nanofibers. These histidine-rich proteins form coacervates with low interfacial energy and shear-thinning behavior that affect the mechanical properties. [22, 72] These histidine-rich proteins further crosslink with catechol compounds, stiffening the network. Cross-linking also contributes to the desorption of water molecules from chitin, which also enhances the stiffness of the beak. [10]

Chitosan-Based Materials Reinforcement Chitosan, the highly deacetylated form of chitin, has gained lots of traction due to its water-processability. Together with its biocompatibility and abundance, chitosan is an attractive candidate for many applications. However, the water processability also comes with diminished

mechanical stiffness and strength. Numerous attempts were made to improve its mechanical strength by either blending chitosan with other polymers[73, 74], or more directly, by chitosan[22, 75-77] cross-linking. Former routes failed to make a significant improvement of the mechanical strength, though adding a plasticizer does improve the composite's ductility. Cross-linking electro-spun chitosan nanofibers with glutaraldehyde[76] does not necessarily improve the stiffness or strength either. Alternatively, phenolic compounds could induce the cross-linking reaction, where oxidized catechol groups form covalent bonding with the primary amine groups of chitosan.[22] There is, however, a lack of systematic studies on how the extent of dopamine cross-linking will affect the mechanical properties of such composites. Thus, building on previous works, I followed the tanning induced cross-linking chemistry inspired by squid beaks, and demonstrated a simple water-processable chitosan-L-dopa composite (ChitoDX) (Fig. 2.1.1a) by cross-linking chitosan with L-dopa. ChitoDX has spatially controllable mechanical properties by simply varying the ratio of the components (Fig. 2.1.1b).

2.2 Experimental Methods

Synthesis of Cross-linked ChitoDX Chitosan (medium molecular weight, Sigma Aldrich) is dissolved at 1% w/v in 0.5M acetic acid (ACS grade, EMD Chemicals) solution. We prepare films with different L-dopa (Sigma Aldrich) and sodium periodate ($NaIO_4$) (ACS reagent, Sigma Aldrich) content -- ChsDXNY, where X is the weight percent of L-dopa and Y is the weight percent of $NaIO_4$ against chitosan respectively. Appropriate amounts of L-dopa are added into the chitosan

solution to achieve the desired composition. The solution is stirred until clear. Corresponding amounts of $NaIO_4$, are added and stirred for 5 minutes. The solution is then poured into a 60 mm petri dish and placed on a hot plate at 50°C overnight to allow solvent evaporation. The resulting film is submerged in 4% w/v NaOH (ACS grade, Fisher Chemical) to neutralize the protonated amine groups in the chitosan and to prevent film dissolution in water during washing[78]. The films are then washed extensively with deionized water to remove any NaOH, and dried at room temperature overnight. The final films have a thickness around 20 µm. As a proof of concept, a gradient film is fabricated by dropping 5 ml solutions of ChsD5N0, ChsD5N1, ChsD5N3 and ChsD5N5 side by side onto a rectangular

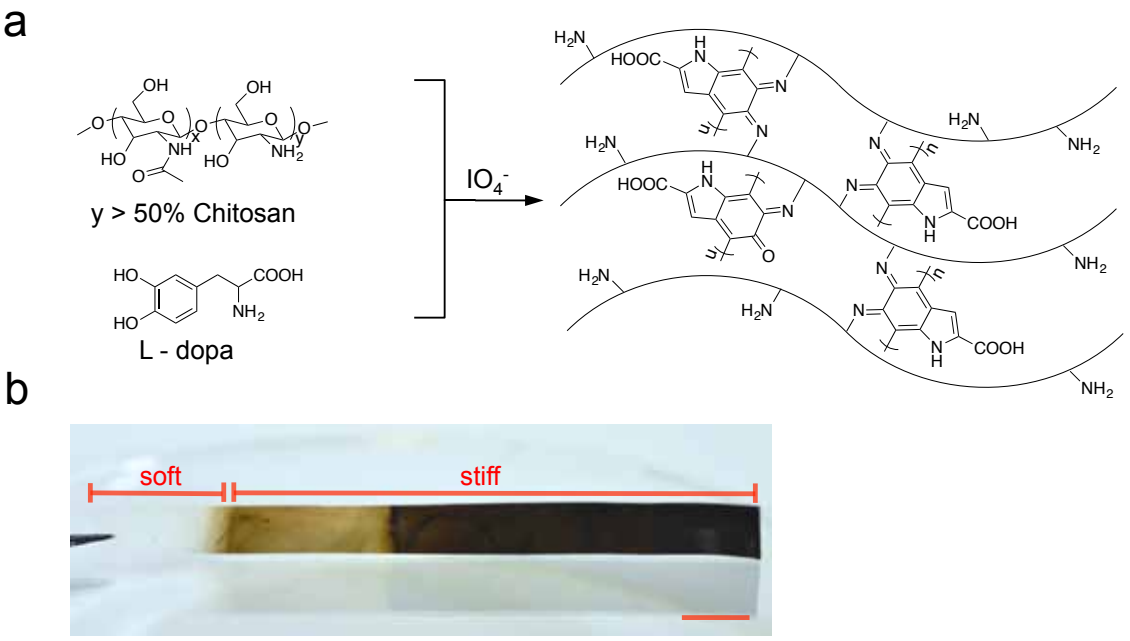

Figure 2.1.1 (a) Brief reaction scheme where L-dopa is oxidized and chemically cross-linked with chitosan, (b) Optical image of synthesized ChitoDX film with varied oxidant composition resulting in different shades of tanning gradient, scale bars: 1cm.

plain glass slide spreading about equal length, followed by solvent evaporation, NaOH treatment and drying processes the same as described above.

Materials Characterizations Ultraviolet-Visible (UV-Vis) spectra are recorded with a Thermo Scientific Evolution 300 UV-Vis spectrometer (300-600 nm, 4 nm resolution). Fourier Transform Infrared (FTIR) spectra are recorded with a Bruker vertex 33 FTIR spectrometer (4000-400 cm^{-1}, 4 cm^{-1} resolutions). Tensile tests are performed with a Shimadzu AGS-X (1 mm/min rate) equipped with a 100 N load cell and 50 N pneumatic grips at room temperature. Tensile testing is repeated with three rectangular samples (5*40 mm, thickness of approximately 20 um) of all materials fabricated. All samples are dried and stored at room humidity, which is monitored with a digital traceable hygrometer (Fisher Scientific). The humidity is consistent around 40% relative humidity. For hydrated tensile tests, samples are first submerged in DI water for 24 hours and tensile measurements are conducted at 65% relative humidity.

2.3 Processing of ChitoDX

To create ChitoDX, we cross-link chitosan with L-dopa using sodium periodate ($NaIO_4$) as an oxidizing agent in a one-pot water-based approach (Figure 2.3.1a). L-dopa first oxidizes into quinone-containing residues in presence of $NaIO_4$ (Figure 2.3.1b). The quinone groups then covalently bond to the amine groups in the chitosan D-glucosamine units, via either Michael-addition[22, 79, 80] (Figure 2.3.1c) or Schiff-base reaction (Figure 2.3.1d). [22, 76] At the same time, when exposed to oxidant, L-dopa also goes through self-polymerization, forming polydopamine-like compounds[81] (Figure 2.3.1e). L-dopa is a

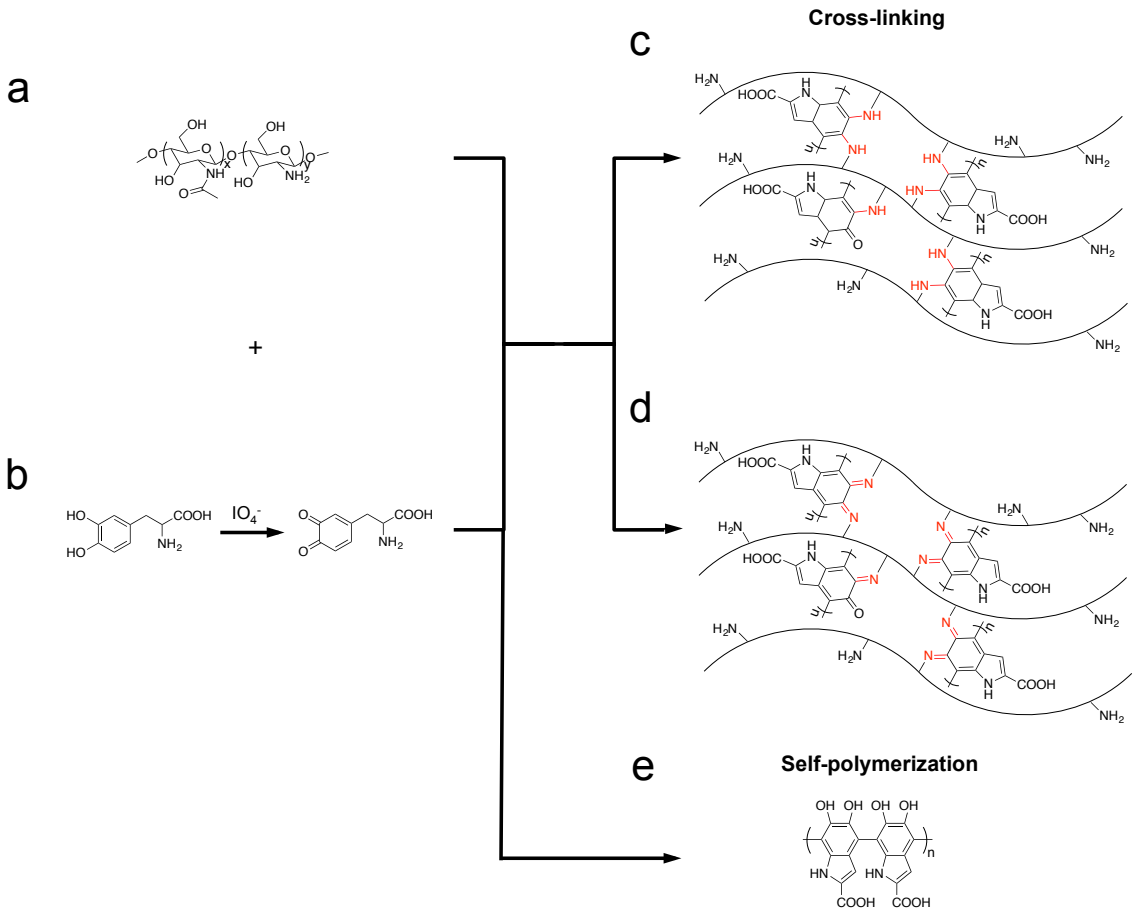

Figure 2.3.1 Reaction cascade where (a) amine groups in chitosan cross-link with (b) L-dopa quinones through an oxidation reaction initiated from sodium periodate via either (c) Michael addition or (d) Schiff base reaction, meanwhile (e) the periodate oxidation also induces L-dopa polymerization into polydopamines.

relatively small molecule compared to chitosan and diffuses faster, thus L-dopa polymerization competes with the cross-linking reaction. In nature, such cross-linking is typically enzyme-catalyzed.[82] Researchers have also demonstrated an incubation-based Tyrosinase-catalyzed reaction[17, 80] and electrochemistry-initiated cross-linking.[83-85] Instead of first grafting catechol groups onto chitosan side chains before cross-linking,[86] here, we choose a direct oxidant-induced route for ease-of processing. ChitoDX is a fully organic amorphous composite. To tune the mechanical properties of ChitoDX, we

prepare films with different L-dopa and $NaIO_4$ contents ChsD5N1, ChsD5N3, ChsD5N5 for further chemical and mechanical analysis.

2.4 Cross-Linking Chemistry of ChitoDX

I perform UV-Vis spectroscopy to study effects of varying L-dopa and $NaIO_4$ ratio on the chemical structure of the composite (Fig. 2.4.1). First, we vary L-dopa concentration with a constant amount of $NaIO_4$ (Fig. 2.4.1a). Higher L-dopa concentrations in the composite results in higher absorbance in the 300-500 nm region. The region between 300 nm and 320 nm corresponds to several L-dopa oxidation intermediates in the cross-linked ChitoDX films. [22, 80, 87] Increasing the L-dopa content from ChsD5N3 to ChsD20N3 also results in higher absorbance in the 420 nm region, the characteristic peak for polydopamine. This increase indicates that the additional L-dopa reacts and polymerizes to form polydopamine. [88] Second, we vary the $NaIO_4$ concentration with a constant amount of L-dopa (Fig. 2.4.1b). Similar to increasing the L-dopa concentration, increasing the

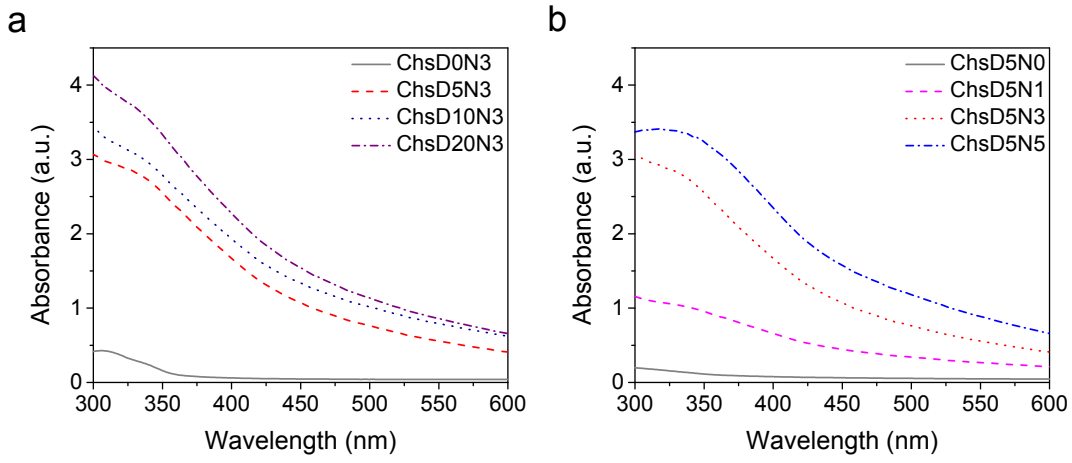

Fig. 2.4.1 UV-Vis spectra for ChsDXNY composites with (a) ChsDXN3 with L-dopa increments and (b) ChsD5NY with oxidant increments.

amount of $NaIO_4$ from ChsD5N1 to ChsD5N3 leads to stronger absorbance in the 300-320 nm region. This higher content of L-dopa oxidation residue conversion also results in the samples prepared with higher $NaIO_4$ content turning from light yellow to dark brown (Fig. 2.1.1b). Since more L-dopa molecules are oxidized and available to cross-link amine groups of chitosan, the L-dopa-chitosan cross-linking density increases. This finding suggests that in ChsD5N1 the cross-linking reaction may not go to completion. An added amount of oxidant will lead the L-dopa to react further, where more L-dopa intermediates are formed. Further increasing the amount of $NaIO_4$ from ChsD5N3 to ChsD5N5 leads to a smaller change in absorbance in the 300-320 nm region. This indicates that the cross-linking reaction is only limited by oxidant content up to a L-dopa/$NaIO_4$ ratio of 1:3. For, ChsD5N5 the excess $NaIO_4$ may lead to oxidization and depolymerization of the chitosan backbone.[89] (Fig. 2.4.2)

2.5 Mechanical Properties of ChitoDX

Elastic Modulus and Tensile Strength of ChitoDX. We explore how varying L-dopa and $NaIO_4$ affects the mechanical properties of ChitoDX (Fig. 2.5.1). For

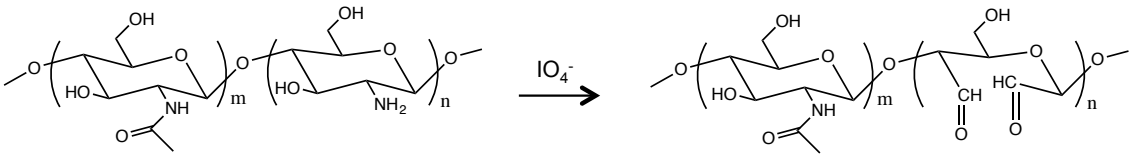

Figure 2.4.2 Periodate ion attacks the amine groups of chitosan, and chitosan becomes partially oxidized.

both ChsDXN1 and ChsDXN3 series, we find the elastic modulus first increases and then decreases when an excessive amount of L-dopa is added to the reaction cascade. For example, the elastic modulus almost doubles, from 2.7 GPa for ChsD0N3 to 4.5 GPa for ChsD5N3 (Fig. 2.5.1a), likely due to chitosan-L-dopa cross-linking into a tightly connected network. As L-dopa concentration further increases from ChsD5N3 to ChsD10N3 and ChsD20N3, the elastic modulus decreases. The cross-linking between L-dopa and chitosan approaches a plateau; further adding L-dopa induces a significant amount of polydopamine formation (Fig 2.3.1e). The formation of such softer polydopamine chains therefore decreases ChitoDX elastic modulus. [90]

The ultimate tensile strength has a similar trend (Fig. 2.5.1b). ChsD0N3 has a strength of 90 MPa, whereas, the tensile strength for ChsD5N3 reaches 190 MPa. The latter is 1.5 times higher than the value for shrilk laminates,[78] and is three times the strength comparing with chitosan alone. Apart from the bulk property of natural polymers and polymer composites, due to a low density of 1.4 g* cm^{-3}, ChitoDX has a specific strength up to 150 MPa/(Mg/m^3). In an Ashby plot[91], ChitoDX compares favorably with natural polymers and polymer composites. The specific strength of ChitoDX is competitive with most natural ceramic composites, the value of which is twice the specific strength of typical aluminum alloy such as 6063-T5[92], and three times that of natural biomineralized composites such as enamel.[91] Toughness for ChitoDX is largely improved (Fig.2.5.1c) Upon cross-linking, ChsD5N1 obtains toughness as high as 50 J/m^3**.** Increasing concentration

of $NaIO_4$ for composite with less L-dopa then ChsD20NX reduces the mechanical properties likely due to oxidation of chitosan backbone. (Fig. 2.4.2) [89, 93]

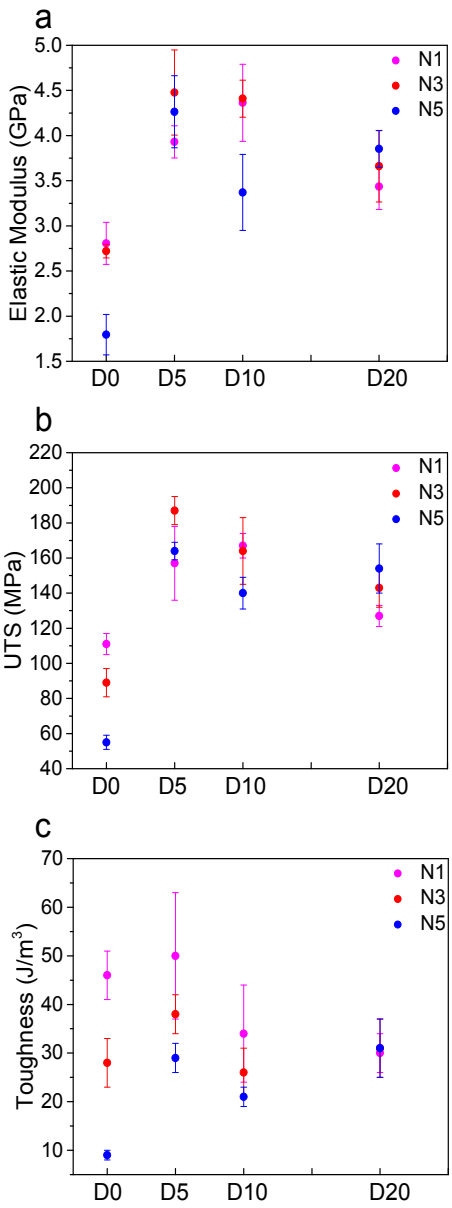

Figure. 2.5.1 Mechanical properties of ChsDxNy composites, including (a) elastic modulus, (b) ultimate tensile strength, and (c) toughness obtained from engineering stress-strain curve of the composites.

To quantify the degree of cross-linking in ChitoDX we monitor the amount of amines on the chitosan consumed by the reaction using FTIR[94] and correlate these amounts with mechanical properties (Fig. 2.5.2). In ChsD5NY, as $NaIO_4$ concentration increases, more amines on the chitosan are consumed in the reaction with a steady increase between ChsD5N0, 1, and 3 and a plateau for ChsD5N5 (Fig. 2.5.2a). Up to ChsD5N3 the decrease in primary amines in the chitosan correlates well with the increase in elastic modulus and tensile strength indicating that the amines in the chitosan are indeed consumed in the cross-linking reaction with L-dopa (Fig. 2.5.2b,c). However, the elastic modulus and tensile strength for ChsD5N5 are smaller than for ChsD5N3 despite a 9% decrease in primary amine content in the chitosan backbone. These amines are likely consumed by the oxidant in chitosan degradation reactions as discussed in the previous section.

Elastic Modulus Under Hydration and Gradient. We further investigate the elastic modulus of ChitoDX under hydrated conditions (Fig. 2.5.2d). We perform uniaxial tensile tests on ChsD5NY samples that are kept in DI water for 24 hours. Adding L-dopa without cross-linking results in an elastic modulus for ChsD5N0

a

Materials	Oxidant wt%	Amine % After Reaction	Change in Amine Content (%)
ChsD5N0	0	83	0
ChsD5N1	1	75	7
ChsD5N3	3	68	13
ChsD5N5	5	61	25

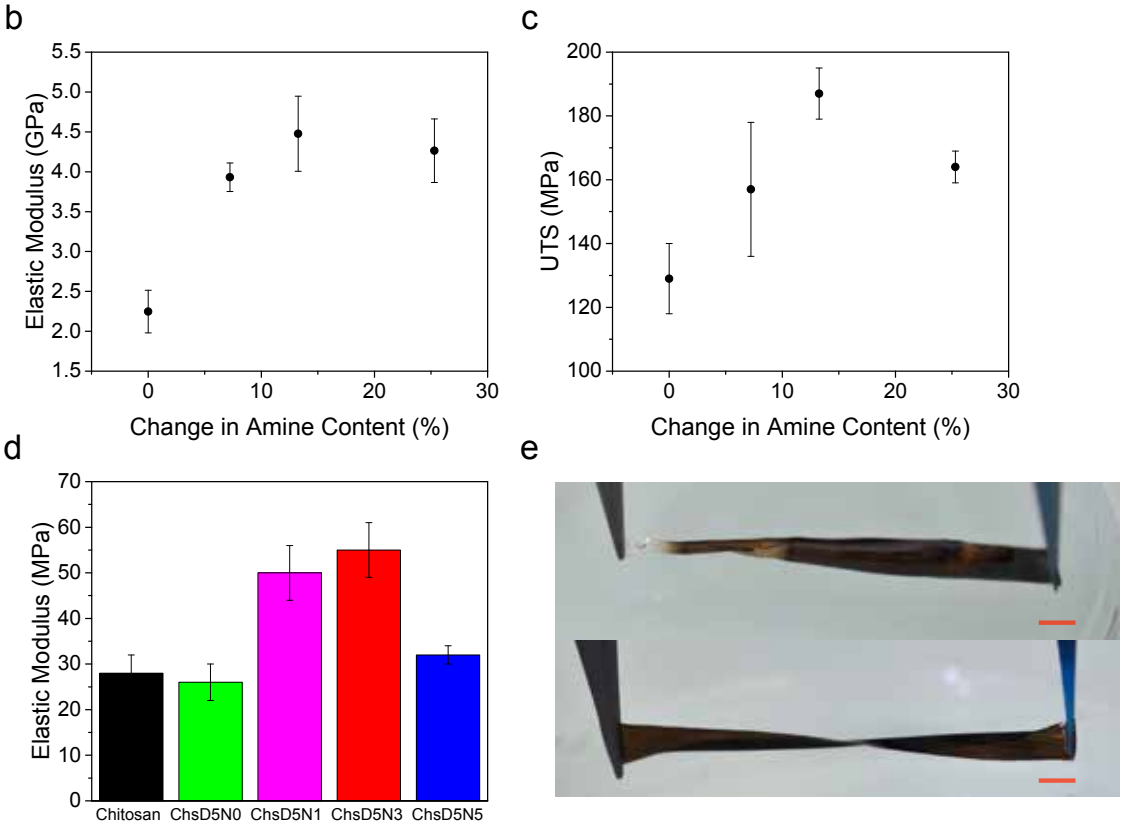

Figure 2.5.2 (a) Table of quantitative analysis of change in NH_2 content among the cross-linked ChsD5NY composites based on FTIR spectra. Mechanical characterization of (b) elastic modulus and (c) ultimate tensile strength for ChsD5NY composites under dry conditions. (d) Elastic modulus for hydrated ChsD5Ny (e) Twisting by one turn of hydrated cross-linked ChsD5NY gradient film (top), and a uniformly cross-linked ChsD5N3 film (bottom), scale bars: 1cm.

that is lower than chitosan. We hypothesize that the presence of small L-dopa molecules within ChsD5NY reduces the interfacial friction[95] allowing the entangled chitosan chains to slide and become aligned more easily under tension. Increasing cross-linking density in ChsD5N1, ChsD5N3 increases the elastic modulus as expected. The wet elastic modulus for ChsD5N3 is as high as 55 MPa, twice the elastic modulus of chitosan (28 MPa) or uncross-linked composite (26 MPa). To mimic the mechanical gradient in the squid, we create a ChsD5NY sample with different concentrations of $NaIO_4$ along its length (Fig. 2.5.2e). The areas exposed to a higher amount of oxidant are darker brown as expected by a larger amount of cross-linking and L-dopa polymerization. To visualize this gradient in elastic modulus, we perform a one-turn twist on hydrated films with and without gradient. For the gradient film (Fig. 2.5.2e, top panel), the twist is concentrated on the softer end of the strip. In contrast, under the same twisting conditions, for a uniformly cross-linked ChsD5N3 film (Fig. 2.5.2e, bottom panel), the twist sits in the center of the strip.

2.6 Conclusions

The cross-linked ChitoDX introduced here utilizes simple one-step cross-linking chemistry initiated by $NaIO_4$-induced L-dopa oxidation. This systematic study provides insights on how to control oxidant-induced L-dopa self-polymerization and chitosan depolymerization to modulate elastic modulus and tensile strength of ChitoDX in both dry and hydrated conditions. Lack of biomineralization in ChitoDX contributes to its lightweight (1.4 g/cm^3) and specific strength of 150 $MPa/(Mg/m^3)$, [92]that ChitoDX is a mechanically efficient materials, sitting at the

upper regime of natural polymer composites in an Ashby plot[91] with tensile strength values competitive to the natural ceramic composites. As an entirely organic and amorphous composite, the mechanical properties of ChitoDX could be further improved by fiber arrangement and inorganic incorporation. With these mechanical properties this composite may find application in bridging mechanically mismatched materials or as a tissue culture substrate to study materials with a mechanical gradient, such as bone to tendon.

It is also worth noticing that an inevitable gap in terms of mechanical tunability still lies between the biological system of squid beaks and the engineered biomimetic composite. A composite of cellulose nanocrystals within a synthetic polymer matrix achieved the soft to stiff transition.[96] Here we also demonstrates a simple method to bridge stiffness mismatch materials by modulate the degree of cross-link. Future work of interest may include bioinspired design at the molecular level.[72, 97]

Chapter III: Chitin Nanofiber Microstructure within Protein Matrix

3.1 Background

Natural structural materials such as insect cuticles, crustacean shells and mollusk nacres often owe their remarkable mechanical properties to the highly ordered organization of chitin nanofiber network embedded within a protein matrix. This hierarchical structure involves several length scales, from the chitin molecular chain alignment, protein wrapped chitin fibrils, sheets of branching network of fiber bundles, to plywood structure composed of these stacked sheets. An extensive optimization of material chemistry has allowed the design of synthetic materials with improved component performance but with limited possibility to engineer their structure across scales. To address this challenge, bioinspired material design strategies are directed towards synthetic materials with combinations of stiffness, strength and toughness at low density by mimicking the hierarchical material organization found in biological materials. In this case, only few practical examples of bioinspired synthetic materials have been reported. The regeneration of high performance natural polymers (e.g. silk fibroin, chitin nanofibers, nanocellulose crystals) into technical materials that can be hierarchically organized across scales represent a paradigm shift that allows fabrication of bioinspired biocomposites using the same components found in the natural materials. In particular, the dual molecular self-assembly and cell-mediated remodeling actions used by nature to hierarchically organize structural biopolymers in living tissues can be mimicked by applying external stimuli at the point of bimolecular self-assembly. It has been shown that chitin can self assemble within a silk matrix, forming into transparent, isotropic

biocomposites from co-dissolve in highly fluorinated isopropanol (HFIP) solutions.[98](Fig.3.1.1) Jin et al have previously demonstrated that chitin nanofibers self-assemble inside a silk matrix yielding a biocomposite, which mimics, on the molecular level, the organic phase of the insect cuticles and the exoskeleton of crustaceans, and demonstrates the improved elastic modulus with respect to that of the separate components alone due to the strong hydrogen bonding between chitin and silk. To this end, I am expanding upon the work by first understanding the localized molecular interaction by visualization through the elastic modulus mapping, and then exploration of the use of electric field-assisted gelation (e-gel) and water annealing methods to improve the control of molecular morphology. Nevertheless, I will also introduce chitin nanofiber self-assembles into a gelatin methacrylate (GelMA) matrix with outstanding stretchability serving as a potential candidate for tissue engineering applications.

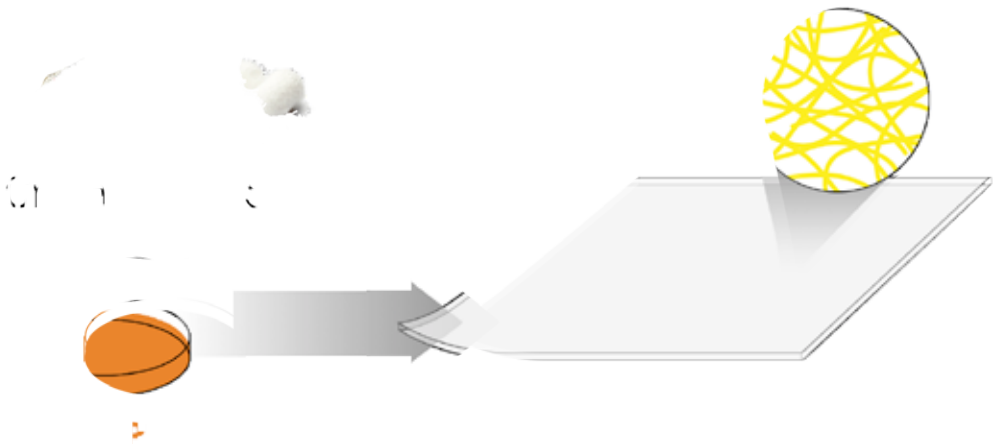

Figure.3.1.1 Schematic illustration showing chitin silk co-assembly process. Squid pen β-chitin and B. mori cocoon silk are co-dissolved in HFIP at various chitin:silk weight ratios. Upon drying, the solution forms a transparent biocomposite comprised of chitin nanofiber of 3nm in diameter self-assembled inside of a silk fibroin matrix. Reproduced from Ref. 98 with permission from Wiley.

3.2 Experimental Methods

Materials Synthesis Silk fibroin and chitin HFIP solutions are mixed in the appropriate ratio (3:1, 1:1, 1:3, in weight ratio) and poured into a cubic PDMS mold. An electric field of 8 V/cm is applied by immersing platinum electrodes in the mold (Figure 3.2.1). A slow evaporation of HFIP is then allowed to drive the sol-gel transition of the mixture. Upon formation of a gel (about 12h), the electric field is removed and the gel-solid transition is achieved by allowing the HFIP to evaporate faster. For water-annealed samples, samples are incubated in a humid chamber at room temperature overnight.

Materials Characterization Fourier Transform Infrared (FTIR) spectra are recorded with Nicolet iS50 FT/IR Spectrometer (4000-400 cm^{-1}, 4 cm^{-1} resolution). Tensile tests are performed according to ASTM D882-12 with a Shimadzu AGS-X (1 mm/min rate) equipped with a 100 N load cell and 50 N pneumatic grips at room temperature. Tensile testing data are repeated with three rectangular samples (5*40 mm, thickness of approximately 20 um) of all materials fabricated. The reported values are average from

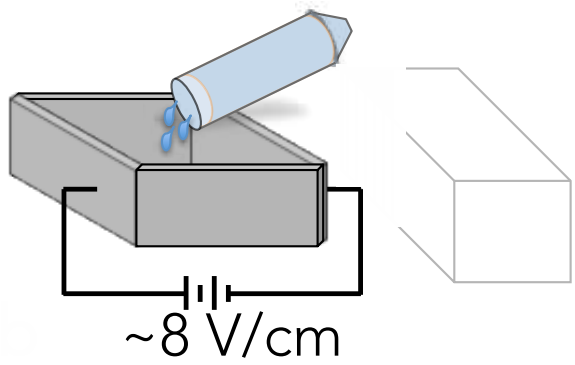

Figure 3.2.1 A schematic showing that an electric field of 8V/cm is applied to assist chitin-silk gelation.

three measurements that according to ASTM D882-12 standard deviation shall not be reported due to the reduced number of data points. All samples are dried and stored at room humidity, which is monitored with a digital traceable hygrometer (Fisher Scientific). The humidity is consistent around 40% relative humidity. Fast Force Mapping mode Atomic Force Microscopy (AFM) was performed on an Asylum MFP-3D Infinity System. Bruker Sb-doped Si cantilevers (ρ= 0.01-0.025 Ω-cm, k = 42 N/m, ν~ 320 kHz) were used on the prepared samples.

3.3 Investigation on Localized Elastic Modulus of Chitin-Silk Biocomposite

Chitin nanofiber self-assemble inside a silk matrix with strong hydrogen bonding interaction. The mechanical performance of such a chitin-silk biocomposite is supposed to follow the rule of mixture, and sits in between the upper limit of chitin and lower limit of silk. The elastic modulus for CS11 composite is 2.5GPa, while pure chitin is 2.3GPa and pure silk is 0.8GPa. The slight increase in elastic modulus of CS11 in comparison of chitin alone is likely due to the strong hydrogen bonding. However, it is known that tensile testing on a macro-scale involves errors resulting from materials defects during processing. Uneven sample thickness during drop-casting, and impurities or minor defects in the composite are just two examples that could lead to early sample failure. Thus, apart from the macro-scale tensile testing, it is essential to find other ways, which are capable of collecting localized mechanical information and characterizing the intrinsic properties of materials. This is also necessary in order to provide a more direct interpretation of the molecular interactions.

Compared to tensile testing, Atomic Force Microscopy (AFM) is one viable way to co-localize topographical information together with mechanical information through mapping technique. In brief, individual force curves can be collected at discrete sites within a region of interest. Depending on the scanning size and number of sites collected, a high-resolution force mapping can be challenging since it may require long testing time. Here, with the Fast Force Mapping Mode (FFM) improved by Asylum Research, a scan of 1um for CS11 film is completed within *c.a.* 30 minutes providing valuable localized elastic modulus information. (Fig.3.3.1) Here it is shown that the elastic modulus spans from ~3GPa to ~9GPa, where the lower elastic modulus area corresponds to the silk protein rich region and the higher elastic modulus corresponds to the chitin rich region. In particular for this AFM scanning method, since a modified contact mode is utilized, during the FFM, the cantilever was touching the surface at a constant force. Thus for Fig.3.3.1b, the possibility cannot be eliminated that when more materials are co-localized

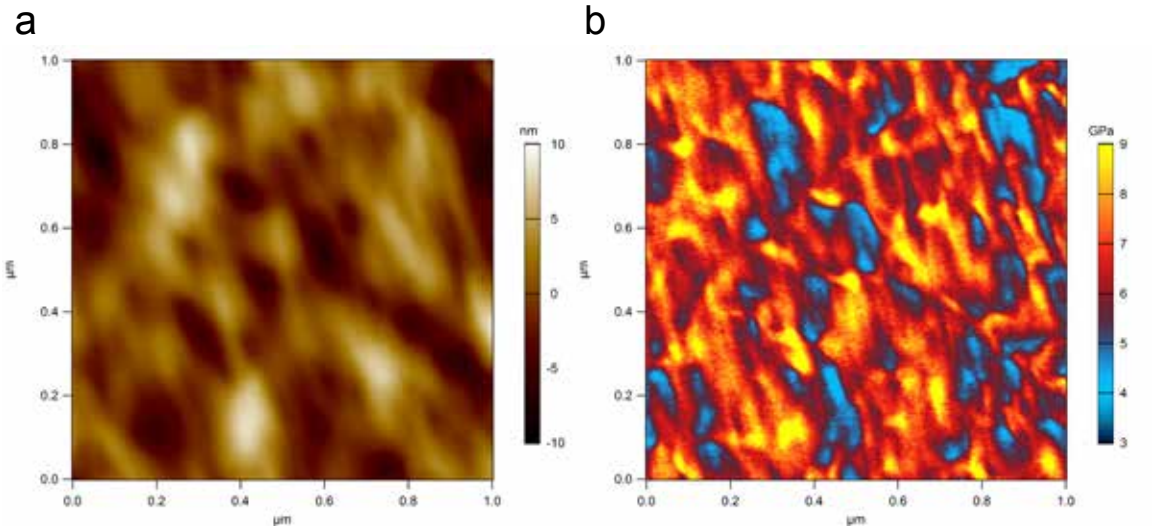

Figure 3.3.1 Atomic Force Microscopy scan of CS 11 (a) topography and (b)elastic modulus mapping

in the same area, a higher elastic modulus might be observed.

3.4 Self-Assembled Chitin-Silk Assembly via E-field Assisted Gelation and Water Annealing

Processing method is a key factor that dictates molecular structure of materials. Previous study done by Hassanzadeh et al have shown that the processing method, drying time and solution concentration could affect chitin nanofiber morphology and density, and, therefore, its mechanical properties.[61] To this end, further studies were carried out to fine-tune the molecular organization of chitin-silk composites.

From a synthesis/processing perspective, several approaches have been carried out such as the application of shear flow,[99] magnetic fields,[100] and electric fields.[101, 102] Electric fields have been widely used to control a materials organization, such as polarizable nanoparticles,[103] nanowires,[104] nanotubes,[105] and individual DNA molecules.[106] Controlling these fundamental building blocks and creating a highly ordered structure on the nanoscale holds great significance for engineering functional materials. Stupp et al have synthesized a group of triblock molecules with one 3,5 dihydroxy-benzoic ester dendritic segment, one rigid rod-like segment and various flexible coil-like segments, referred to as DRC molecules. These DRC molecules were self-assembled with the aid of an AC field, where the supramolecular assemblies align with the electric field.[102] DC fields have also been used to assist in the alignment of supramolecular fibers. A cyclohexane trisamide gelator first self-assembles into supramolecular fibers in an organic solvent, and then deposited between two gold electrodes while applying a DC

voltage. The DC voltage triggered the alignment of these supramolecular fibers in preferred directions aligning with the electric field.[101]

To this end, using electric fields as an external stimulus to facilitate fibrous network organization becomes an interesting topic, particularly in its potential to achieve anisotropy properties. Thus, in collaboration with Professor Omenetto at Tufts University, I start to explore how a DC voltage applied during gelation could potentially affect the molecular structure of chitin-silk biocomposite.

Based on the hypothesis for chitin nanofiber alignment with the aid of electric field, anisotropy would be expected, which would lead to a difference in the elastic modulus and tensile strength of materials according to the rule of mixture. Thus, tensile testing is the most intuitive examination method. Here, tensile testing is conducted on e-gel

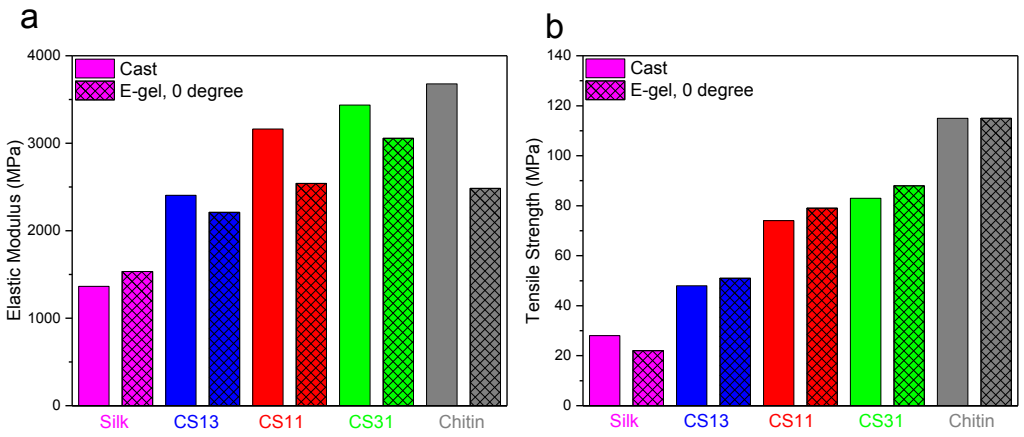

Figure 3.4.1 (a) Elastic modulus and (b) tensile strength of chitin-silk composites using drop-casting and e-gel method respectively.

samples as well as drop-casted samples as a control at room temperature and humidity. Define 0 degree as the axial loading, where the direction of tensile pulling is along with the applied electric-field direction. According to composite theories that the elastic modulus is expected to increase when pulling along the axial direction with respect to its isotropic elastic modulus, while decrease with a transverse direction loading. There is no increase in elastic modulus for the electric-field-assisted gelation (E-gel) samples as it is shown in the Figure 3.4.1 (a). For chitin-silk composites, the elastic modulus increases as the concentration of chitin increases in the composites. It is worth noticing that here CS31 has a higher elastic modulus than chitin alone, which indicates a new phase of hydrogen bonding is formed between chitin and silk.[98] The tensile strengths for E-gel samples are about the same as compared to the casted samples. These results, in particular the results of elastic modulus, indicate that there is a lack of anisotropy in the chitin-silk composites.

This finding is further confirmed by comparing the mechanical properties between axial (0 degree between the loading direction and the applied electric-field direction) and transverse (90 degree between the loading direction and the applied electric-field direction) tensile loading conditions. According to the composite theory, by pulling along the fiber alignment direction, the fiber sliding mechanism becomes dominant and promotes plasticity. In comparison, the transverse loading would accelerate material failure. Here taking CS31 as an example, (Fig. 3.4.2) there is no significant change when applying the tensile load in an axial or transverse fashion, which also indicates that there is no preferred fiber orientation within the chitin-silk composite by using this electric-

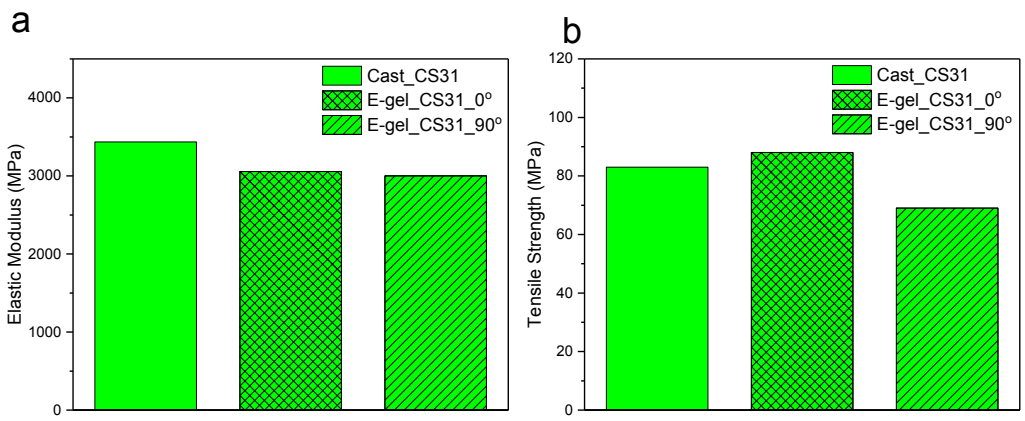

Figure 3.4.2 (a) Elastic modulus and (b) tensile strength of CS31 composite with drop-casted method or e-gel by applying tensile load either 0 degree or 90 degree between the loading direction and the electric-field direction.

field-assisted gelation method.

Despite a lack of preferred fiber orientation, an increase in ductility, leading to improved toughness is observed within e-gel samples (Fig. 3.4.3) Take CS31 for example. The E-gel sample has a strain of 10% while the casted sample of about 3.5%. (Fig. 3.4.3a) This leads to the increase in toughness that the E-gel sample has a toughness of 6.8 MPa, three times as high as that of the casted sample (2MPa). To better understand this increase in ductility for electric-field-assisted assembly of chitin-silk composite, mechanical performance of pure chitin and silk are used as a control. While there is not much difference in ductility for pure silk samples using either casting or e-gel, the ductility for e-gel chitin is 3 times as high as that of casted samples. Nevertheless the toughness for E-gel chitin can reach as high as 11.23 MPa. These serve as indicators that during the e-gel assisted assembly, the molecular morphology is fine-tuned.

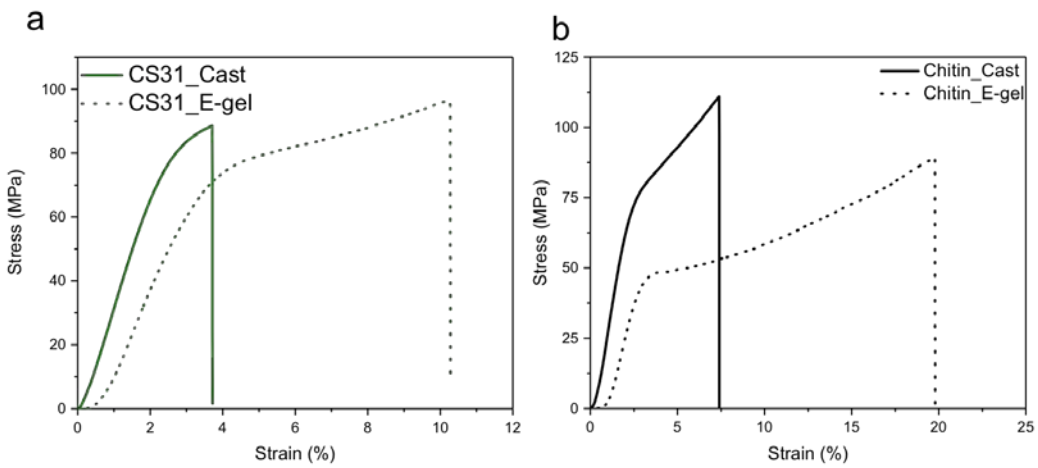

Figure 3.4.3 Stress-strain curves of (a) e-gel processed chitin-silk composites with varied weight ratio, (b) pristine chitin films prepared via either drop-casting or e-gel.

Fourier Transform Infrared Spectroscopy (FTIR) is conducted in order to gain more insights of molecular morphology change by applying the electric field. (Fig. 3.4.4) The three characteristic peaks for hydrogen bonding are analyzed carefully. Amide I corresponds to the hydrogen bonding between C=O group of chitin with the –NH group of an adjacent chitin chain (1657cm^{-1}) and with an –OH group of the same chitin chain (1620cm^{-1}). Amide II (1557cm^{-1}) and Amide III (1310cm^{-1}) correspond to the –NH bending and stretching together with –CN stretching mode. There is a slight increase in intensity for Amide I and Amide II for E-gel CS31, indicating an increase in hydrogen bonding. (Figure 3.4.4 a and b) In particular for Amide III, where there is a split for chitin (1310 cm^{-1}) and silk (1230 cm^{-1}), the intensity for hydrogen bonding in chitin increases while that for silk decreases. Similar trend of increase in hydrogen bonding is also observed for e-gel chitin in comparison to casted ones. A control FTIR scan of silk samples prepared from both drop-casting and e-gel is also performed, that no significant

peak intensity change or shift was observed. Thus, it is speculated that chitin molecular morphology is tuned via e-gel, which then affects the chitin-silk composite molecular morphologies. This suggests that during the electric-field-assisted assembly, there is an increase in the chitin nanofiber entanglement. This increase in entanglement results in more physical cross-links. Thus during tensile testing, when samples undergo plastic deformation, there is a prolonged time is required for the fiber uncoil.[107] This extensive molecule uncoiling thus results in the increased in the ductility.

In addition, the physical cross-link also causes an increase in hydrogen bonding, which could lead to a slip-pulse propagation mechanism during plastic deformation.[108] Localized breaking of intermolecular hydrogen bonds is controlled by the applied tensile stress. During the tensile loading, these hydrogen bonds may be broken one at a time, contributing to the increase in ductility as well.

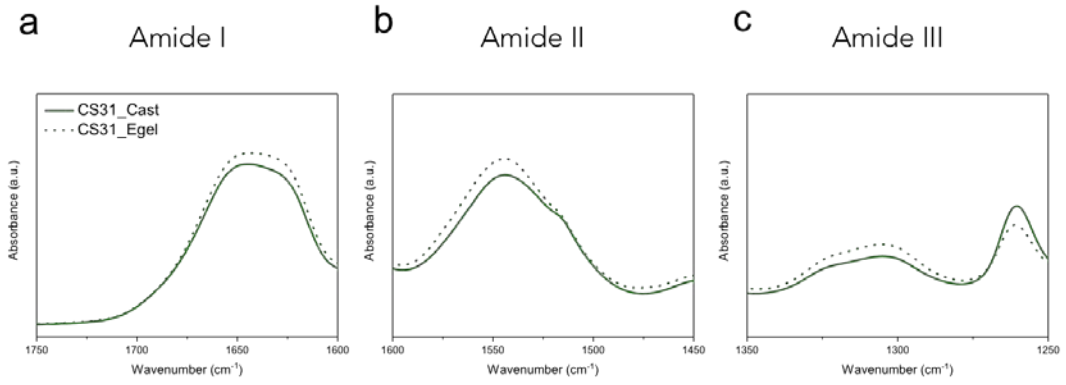

Figure 3.4.4 FTIR spectra of (a) Amide I, (b) Amide II, and (c) Amide III peaks for CS31 samples using casting and electric-field assisted method respectively

Apart from the electric-field-assisted method, water vapor annealing is another route to tune the molecular morphology of chitin-silk composites. The physical structure of fibrous silk proteins can be controlled through temperature-controlled water vapor annealing (TCWVA).[109] This simple water annealing technique can induce crystallinity from α-helix dominated silk I structure at 4°C, to highest content of ~60% crystallinity of a β-sheet dominated Silk II structure at 100°C. Jungho et al previously confirmed that chitin transforms from β-chitin into α-chitin nanofibers; while silk remains in the α-helix conformation (Silk I) from the HFIP solution co-assembly.[98] Silk fibroin protein has two major microstructural forms, Silk I and Silk II,[110] where Silk I refers to the α-helix conformation, and Silk II is the insoluble antiparallel β-sheet crystal confirmation. Here I exploit this simple water annealing approach to induce β-sheet crystallization of silk upon

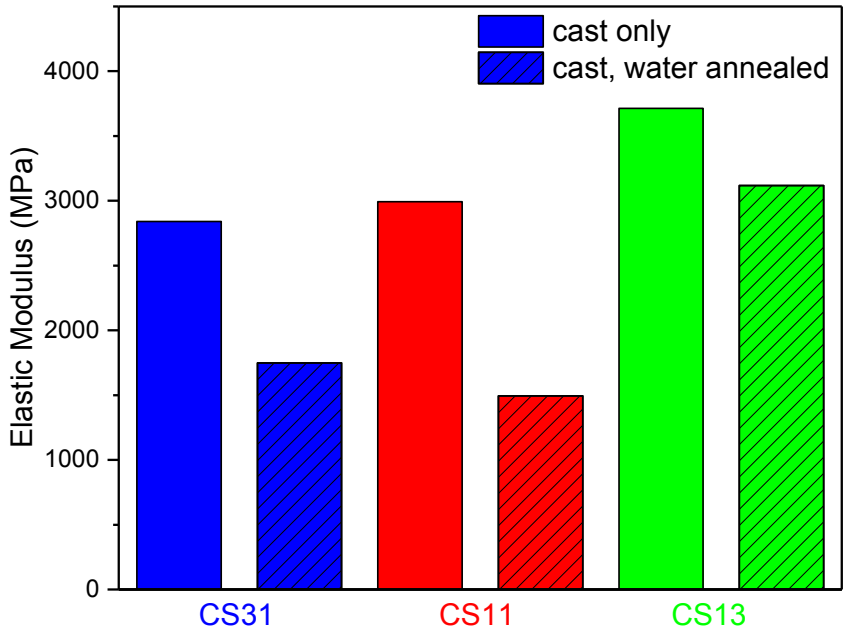

Figure 3.4.5 Elastic modulus of drop-casted chitin-silk composites in comparison with those with water annealing post treatment.

post treatment, and to investigate the microstructure of chitin-silk composite, and its structure-property relationship.

Some preliminary mechanical property characterization has been done to investigate the effect of post treatment on water annealing. (Fig. 3.4.5) Using drop-casted film without post treatment as a control, the water-annealed samples have lower elastic modulus, and have more of a ductile behavior. Such trends suggest that the water annealing process allows extensive molecular chain rearrangement within a humid environment, thus there is more physical entanglement, leading to additional polymer uncoiling during tensile loading.

3.5 Self-Assembled Chitin-GelMA Composite with Cross-linking Reinforcement

Previous work in Rolandi Group has already demonstrated the self-assembly of chitin nanofibers in the matrix of silk fibroin. The microstructure of chitin-silk composites can be tuned by varying relative weight ratios of both components, resulting in a span in mechanical performance. This co-assembly process results in an improved stiffness up to 2 times that of silk fibroin alone and up to 1.5 times that of even stiff chitin films. Based on the chitin-silk assembly, the co-assembly of chitin gelatin became of interest, in order to gain more insights into the chitin-protein molecular interaction in terms of microstructure, processing, and physical and mechanical properties, as well as to serve a proof-of-concept tissue engineering substrate.

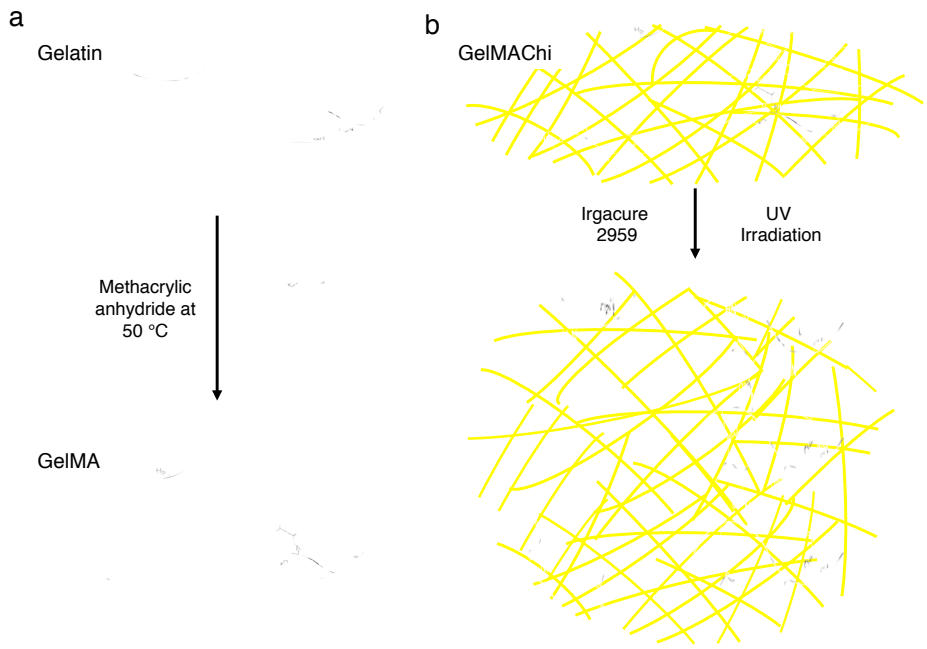

Figure. 3.5.1 Synthesis of (a) gelatin methacryloyl (GelMA) through functionalizing gelatin's primary amine groups by mathacrylic anhydride (MA) at 50 °C, (b) Crosslinked GelMA-chitin (GMAC) films by exposure of dry GMAC films to UV irradiation in the presence of a photoinitiator (PI), Irgacure 2959, for 3 minutes.

One challenge in tissue engineering area is to select a suitable material to serve as the scaffold platform. There are two key requirements in selecting such material. One is to ensure that the materials selected is cellular compatible, or even better, that it contains certain molecular cues that resemble the composition as it is in the extracellular matrix (ECM).[111] The other key component is to ensure that the elastic modulus of the selected material matches with the target tissue type to facilitate cellular development.[112] Here modified gelatin methacrylate is selected as the protein component since it meets both requirements, and thus has gained much traction in the area of tissue engineering and regenerative medicine. Gelatin, a denatured collagen that can be extracted from various

sources retains natural cell-binding motifs, such as RGD and MMP-sensitive degradation sites.[111] On the other hand, modified gelatin methacrylate is a photo-crosslinkable material, resulting in a chemical cross-linked network with UV radiation exposure, with enhanced mechanical stiffness, as well as stability at body temperature. Thus we co-assemble chitin and gelatin methacrylate with the assistance of UV cross-linking for film formation. (Fig.3.5.1)

Chitin nanofibers self-assemble within GelMA and yield GMAC hybrid films with variable chitin nanofiber content (Fig. 3.5.2). The pristine GelMA film is smooth (Fig. 3.5.2a). Increasing the relative concentration of chitin and GelMA in GMAC31,

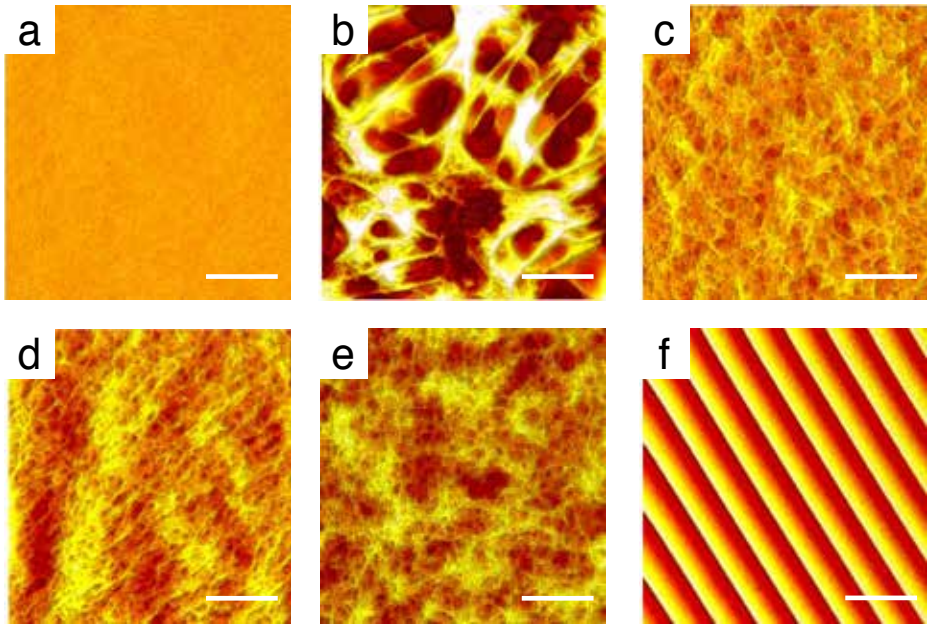

Figure 3.5.2 (a-e) Topographic atomic force microscope (AFM) images of GelMA, GMAC films with different GelMA:chitin weight ratios, and Chitin. GMACXY are GMAC films with XY = GelMA:Chitin weight ratio. (a) GelMA, (b) GMAC31, (c) GMAC11, (d) GMAC13, and (e) Chitin, respectively (scale bars are 500 nm). (f) Topographic AFM image of micro-patterned GMAC13 with a pitch of 12.15 μm and a height of 450 nm (scale bar is 20 μm).

GMAC11, GMAC13 (GMACXY, where X:Y = GelMA: chitin weight ratio) yields films with an increased fraction of chitin nanofibers as expected (Fig. 3.5.2b, c, and d).[47] In GMAC31 (Fig. 3.5.2b), the high amount of GelMA may result in the formation of GelMA agglomerates. In GMAC11 and GMAC13 (Fig. 3.5.2c and d), the chitin nanofibers in the co-assembled hybrid hydrogel have the same entangled structure as the chitin nanofibers self-assembled from a chitin only-HFIP solution (Fig. 3.5.2e) indicating the robustness of chitin nanofibers self-assembly in the presence of GelMA. This microstructure control affords a simple strategy to fine-tune the mechanical properties of GMAC hydrogels. The GMAC films are solution processable and amenable to soft-lithography strategies that we have previously developed for chitin[113] and chitin-silk.[98] Micropatterns with the pitch of 12.15 μm and height of 450 nm are fabricated on GMAC13 using solution-based replica molding (Fig. 3.5.2f) GMAC hydrogels are overall more robust than the GelMA counterparts without chitin nanofiber reinforcement (Fig. 3.5.3). GelMA hydrogels have elastic modulus in the range of 3.3-110 kPa depending on the GelMA concentration and degree of methacrylation.[114] Chitin nanofibers in the matrix of GMAC hydrogels increase the elastic modulus significantly (from 3.3 KPa to 2.8 MPa for GMAC31 and to 4.6 MPa for GMAC11 and GMAC13) (Fig. 3.5.3a). The increase in the elastic modulus for GMAC is due to physical reinforcement of the soft matrix of GelMA with entangled chitin nanofibers. This increase in elastic modulus is more pronounced for GMAC13, which has higher content of chitin nanofibers. While we previously observed strong hydrogen bonding between chitin and silk, [98] GelMA and chitin do not show any substantial hydrogen bonding between the two molecules as indicated by Fourier Transform Infrared (FTIR) spectra.[98]

This low degree of hydrogen bonding between GelMA and chitin might be due to a small number of available amine groups in the highly methacryloyl-modified (>80%) GelMA. These amine groups are required for hydrogen bonding with the C=O in chitin. It is likely that this reduced degree of hydrogen bonding in the GMAC composites causes a decreased elastic modulus from 633.6 MPa for chitin to 4.6 MPa for GMAC with only 10% GelMA (Fig. 3.5.3a). It is conceivable that GelMA position itself between the chitin nanofibers, reducing the intrafiber hydrogen bonding, and acts as a lubricant to yield material with lower elastic modulus than what is expected from the rule of mixtures (Fig. 11a). This lubrication effect affords, on the other hand, a very high strain to failure or extensibility of 224 % for GMAC hydrogels. This strain-to-failure is >100 % improvement with respect to GelMA hydrogels and > 200 % improvement with respect to chitin alone (Fig. 3.5.3b-d). The GMAC11 and GMAC31 hydrogels also stretch 80 % more than chitin (Fig. 3.5.3b).

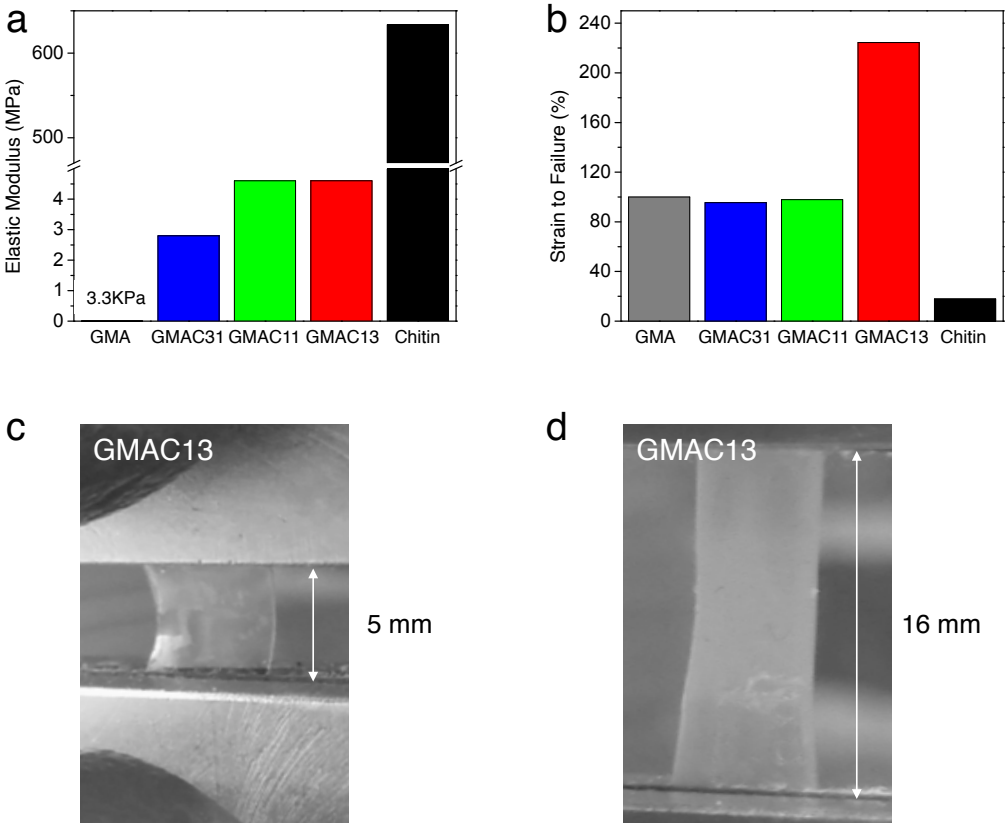

Figure 3.5.3 Mechanical properties of hybrid GMAC hydrogels from tensile test analysis, (a) Elastic moduli obtained from slopes of linear region in engineering stress-strain curves (Figure S4) of the hydrogels with different GelMA:chitin weight ratios. The elastic modulus for all GMAC hydrogels are higher than what has been reported for GelMA and they are lower than chitin alone, (b) Values of engineering strain to failure for hybrid hydrogels with different GelMA:chitin weight ratios. GMAC13 is > 100% more extensible than GelMA and > 200% more extensible than chitin alone, (c) Optical image of GMAC13 at the initial state before load application in mechanical tensile testing, (d) Optical image of GMAC13 showing 224% extensibility under tensile load, showing final length of 16 mm.

Furthermore, GMAC13 is selected for cell cultures because of its higher elastic modulus and superior extensibility. As a proof-of-concept HUVECs/hMSCs are co-cultured on micro-patterned GMAC13 hydrogels in collaboration with Professor Ali Khademhosseini (MIT, Harvard) and Dr. Nasim Annabi (Harvard, Boston University). Here, a higher degree of alignment for micro-patterned GMAC13 substrate is observed as compared to

patterned chitin substrates alone (95% vs 55%). This might be due to the higher flexibility of the GMAC13 substrate, facilitating surface patterning. We also evaluate the viability, proliferation, and vascularization of HUVECs/hMSCs co-cultured on the GMAC13 hydrogels after 1, 3 and 5 days of culture, and suggest that GMAC13 is a novel platform for studying vasculogenesis that is easier to source than Matrigel[115] and more mechanically robust than collagen-based hydrogels [116]. In summery, the chitin nanofibers reinforced GelMA hydrogel is a mechanically robust substrate for tissue engineering applications, which also offers more insights into the structural-performance relationships of chitin-nanofiber-protein-like system.

3.6 Conclusions

In summary, first with the aid of FFM on AFM, localized elastic modulus information is collected to characterize the intrinsic materials property for chitin-silk composite, as well as improve our understanding in the molecular interactions. Building on the previous chitin-silk co-assembly work done in Rolandi Group, two additional methods have been used to fine-tune the molecular morphology. Electric-field-assisted gelation method fine-tunes the microstructure of chitin molecule alone with more β content and added chitin ring stretching. Such a change in molecular morphology provides chitin-silk composite additional ductility and toughness. On the other hand, the water-annealing method is more critical in treating silk components in chitin-silk composite, leading to additional physical cross-link and enhanced ductility. Besides using silk as the protein component, chitin nanofiber self-assembly within a modified gelatin network is also investigated. Chitin nanofibers largely enhance the elasticity of the UV cross-linked gelatin

methacrylate network, and the resulting hydrogel has outstanding strechtability. As a proof-of-concept, Human Umbilical Vein Endothelial Cells (HUVECs) and Human Mesenchymal Stem Cells (hMSCs) are co-cultured on the hydrogel substrates, demonstrating improved cell proliferation and vascularization.

Future research should be focused on the optimization of the electric-field-assisted gelation method by varying the strength of the electric field and the sample distance between electrodes to investigate possibility to align chitin nanofiber within silk matrix, and to further tune the microstructure By building such structural anisotropy, fabrication of a multi-layer, hierarchical laminated structure may become feasible, which could further optimize the mechanical performances of chitin-silk biocomposites. Nevertheless, the capability to align chitin nanofiber within a protein matrix could become a viable method for enhanced cellular alignment as a tissue culture substrate.

Chapter 4: Nature Mineralization in Banana Slug Radula Teeth

4.1 Background

The Mollusca radula is a rasp-like toothed structure used for scraping food into the gut. Depending on species, the morphology and chemical composition of radula teeth vary largely as they may serve different purposes. The radula teeth of chiton, marine mollusks known to graze algae from rocks for food, have been investigated as a model for biomineralization process.[30, 117] The radula tooth of chiton is a highly organized structure of chitin nanofibers imbedded within protein matrix with magnetite minerals. (Fig.4.1.1) Chitin molecules first assemble into a highly crystalline α-chitin nanofiber network, based on which amorphous chitin is permeated within the network to create a rougher surface. This rougher surface facilitates the binding of chitin-binding proteins. These chitin-binding proteins also have an acidic site, which attract either Na^{+} or Mg^{2+} ions to bind these Na^{+} and Mg^{2+} sites then promote the mineralization process with magnetite. (Fig. 4.1.1a) It is reported that the mature chiton tooth has a core-shell structure (Fig. 4.1.1b) with a Ca/P/O-rich apatite core (Fig. 4.1.1 e and f) and a Fe/O-rich magnetite shell (Fig. 4.1.1 c and d). Thanks to the magnetite shell, chiton tooth has an ultrahigh hardness.[30]

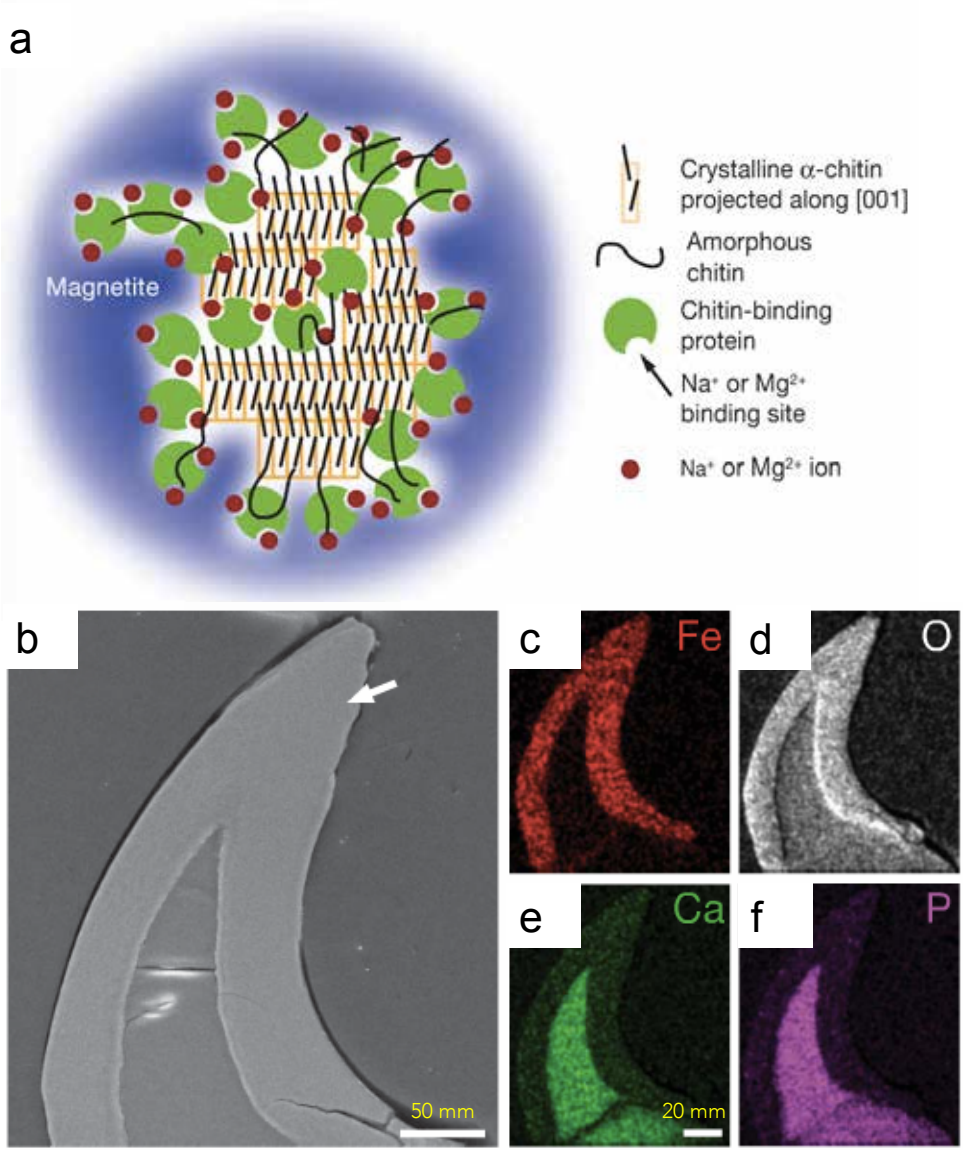

Figure 4.1.1 (a) Model of a chiton tooth organic fiber. b, SEM image of polished cross-section of a tooth. Scale bar, 50 mm. c, Scanning electron microscopy-energy dispersive X-ray spectroscopy (SEM-EDS) elemental maps of cross-section (b) showing a Ca/P/O-rich core (apatite) and Fe/O-rich cap (magnetite). Scale bar, 20 mm. Reproduced from Ref. 70 with permission

Although formation of the teeth has been studied in chiton, very little is known about the radula formation and composition in mollusks that are terrestrial. Banana slugs, terrestrial gastropods in the genus *Ariolimax,* are one such example. (Fig. 4.3.1a) Native

to the Pacific Coast of North America, banana slugs are often bright yellow in color, although some are solid greenish, darker yellow, or even with black spots occasionally. Banana slugs can be as long as six inches in lengths. Both the length and body color could correlate to the banana slug species, aging, habitat and aging. Banana slugs are generally herbivores that they eat most of the leafy greens, mushrooms, and fruits that can be found in the redwoods.[118] This is in particular interesting considering the diet for terrestrial mollusks are mostly leafy greens while chitons need to chew rocks for food. The research interest thus arises from how a difference in diet could affect the teeth morphology and chemical compositions for such terrestrial mollusks. Although the species, natural habitat and evolution history of banana slugs have been studied previously,[119, 120] little is known about the banana slug radula teeth.

Early characterizations on gastropod radula teeth could trace back to 1960, that British species of slug radula is described. The study describes radula as a flexible membrane, on which there are transverse rows of teeth. The form of the teeth in a row varies, and symmetry could be distinguished. To assist understanding, hand-drawing pictures can often be found in the early studies, showing different teeth shapes.[121] Moens and Rassel did a comparative study of three slug species, and found out the fundamental difference in the functioning of three different types of teeth in relation to diet.[122] During feeding, slug radula works as a conveyor belt for food transfer. (Fig.4.1.2) The most anterior row of the teeth gets worn out and breaks off.[123] The teeth are continuously being replaced, and studies have indicated that the younger teeth are very soft, while the further forward ones are hardened.[124] Building on these preliminary understandings, this study is focused

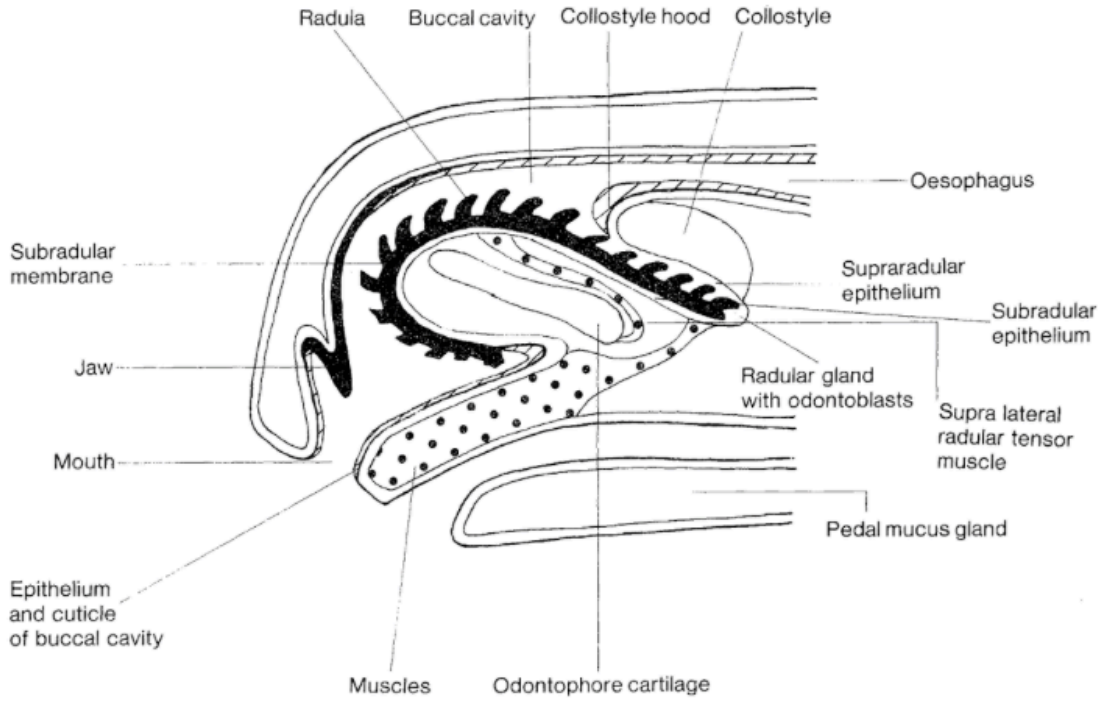

Figure 4.1.2 Anatomy of the sagittal section through the head of a slug. Reproduced from Runham and Hunter (1970)

on banana slug radula teeth. First I will provide a detailed explanation of radula tooth shape, which is position-dependent, with the aid of optical imaging and Scanning Electron Microscopy (SEM). Then I will show the chemical composition of radula teeth, from the organic matrix to the mineralization. At the end, I will introduce the preliminary findings that the mineralization component on a single tooth is position-dependent as well.

4.2 Experimental Methods

We received frozen banana slugs from our collaborators at the Institute of Marine Science, UCSC. These slugs were collected at the Purisma Creek Redwoods Preserve

near Half Moon Bay, and were humanely anesthetized and put down in carbonated water before freezing. Frozen slugs were first thawed in water at room temperature. To extract the banana slug radula, the whole slug was dissolved in 1M NaOH solution overnight. The radula was then picked up from the solution, and washed three times with DI water. Optical Images were taken with a Keyence Digital Microscope VHX-6000 series. Fourier Transform Infrared (FTIR) spectra are recorded with Nicolet iS50 FT/IR Spectrometer (4000-400 cm^{-1}, 4 cm^{-1} resolution). For Scanning Electron Microscopy (SEM) images, samples were first dehydrated with 25%, 50%, 75% and 100% ethanol step-wise. The samples were then mounted on the SEM stub with carbon glue, and went through carbon coating. SEM images were taken with FEI Helios 600i Dual Beam FIB/SEM at 1kv. EDX scanning was conducted with the Octane Silicon Drift Detector that is attached to the Helios system, and at an accelerator voltage of 20keV.

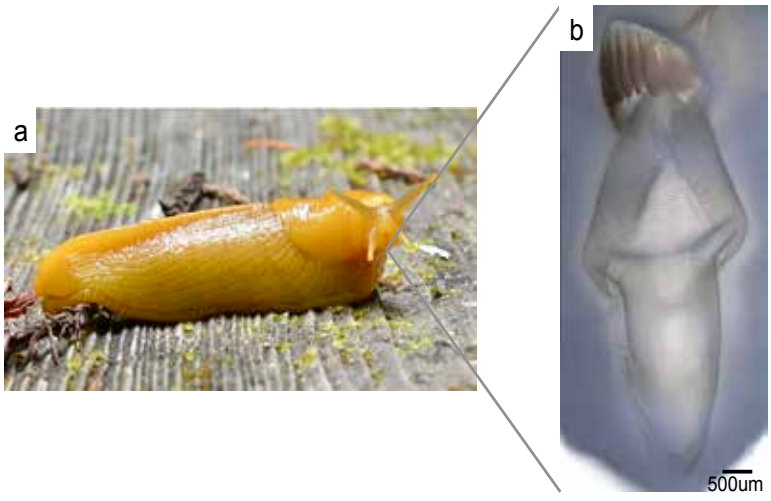

Fig. 4.3.1 (a) Photograph of a banana slug *Ariolimax* (b) Optical image of the banana slug radula with the jaw attached.

4.3 Radula Tooth Characterizations

The extracted radula is first observed under optical microscope. (Fig. 4.3.1b) The banana slug radula is a conveyor-belt like structure. Banana slug radula comprised of transverse rows of teeth with files pointing in longitudinal directions. Unlike the chiton, with only one pair of teeth on each row, there are dozens of teeth on each row for banana slug radula. Interestingly center symmetry was observed for this radula. (Fig. 4.3.2) Depending on their specific position, teeth on the same row are being sorted in three categories – medial, lateral and marginal – each are of different shapes. (Fig. 4.3.2a-d) The medial tooth sits at the center symmetry with two shoulders. (Fig. 4.3.2a,c) On either

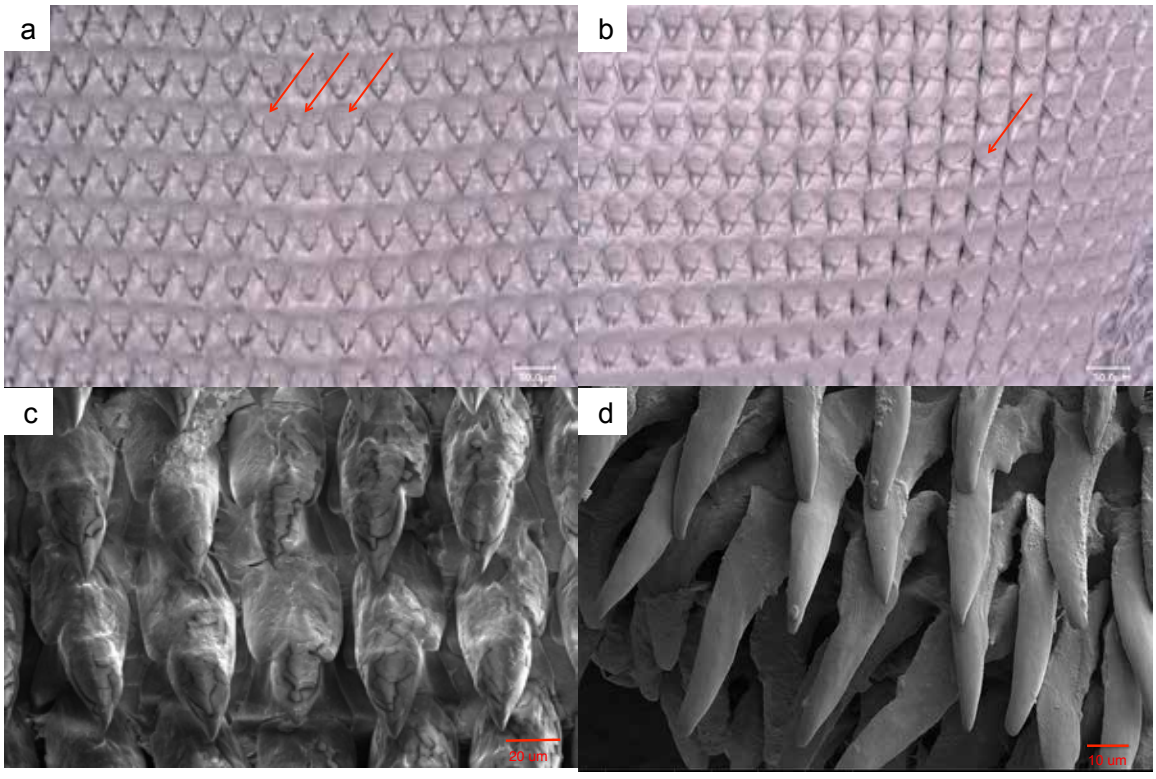

Figure 4.3.2 Optical image of banana slug radula teeth displaying high symmetry of the teeth from (a) the center to (b) the edge. Zoom-in SEM images of radula teeth showing different shapes depending on specific teeth position, (c) medial and lateral, (d) marginal.

side of the medial tooth are the lateral teeth, with only one shoulder. (Fig. 4.3.2a,c) When progressing to the edge of a radula, the shoulder diminishes and becomes a tooth with high aspect ratio, which is the marginal tooth. (Fig. 4.3.2b,d)

4.4 Chemical Analysis

In order to confirm the chemical composition of the banana slug radula, a Fourier Transform Infrared Spectroscopy (FTIR) was conducted in order to investigate the organic component of the banana slug radula. (Fig.4.4.1) Chitin is identified in the

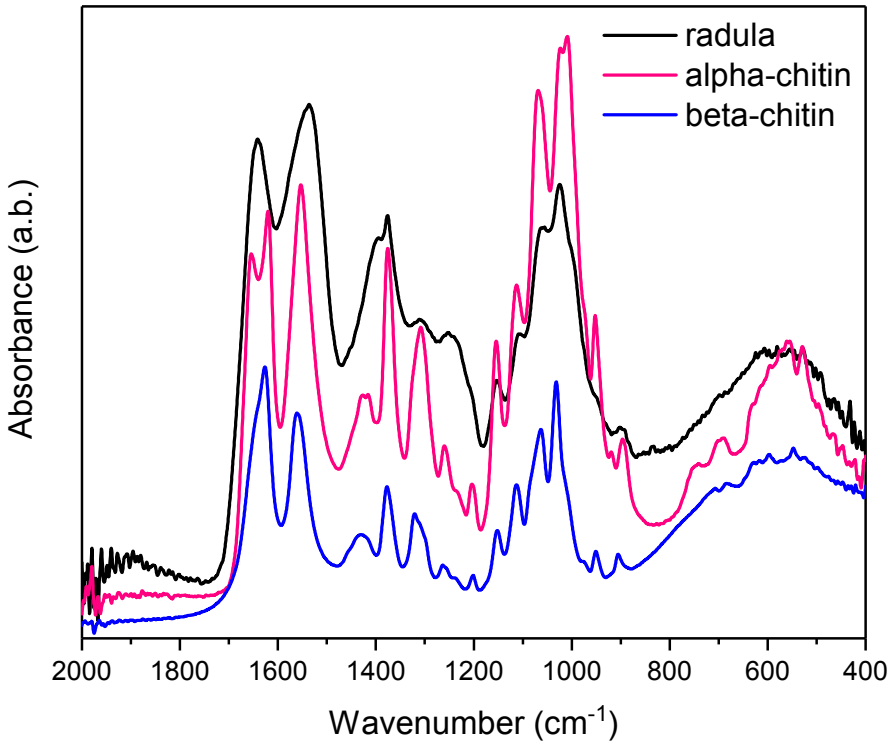

Figure 4.4.1 Fourier Transform Infrared Spectroscopy (FTIR) scan of banana slug radula teeth in comparison with α-chitin and β-chitin.

banana slug radula according to the characteristic peaks from pure chitin as a control. Importantly, unlike chiton radula where a large amount of α-chitin is present, β –chitin is identified here in the banana slug radula. As seen from the spectra, instead of the amide-I (C=O stretching) split peaks at 1657 cm^{-1} and 1620 cm^{-1}, there is only one peak at 1635 cm^{-1}, which confirms β –chitin presence.

Taking a higher magnification of the SEM, different surface morphologies of the banana radula teeth were observed. (Fig. 4.4.2) For tooth closer to the jaw, there is a plate-like structure on the surface, (Fig. 4.4.2a) while, in comparison, the tooth farther away from the jaw lacks such surface morphology. (Fig.4.4.2b) Also, it is noticed that tooth size also varies depending how their longitudinal position. In Figure 4.4.2a, the image only shows the center part of a medial tooth, where its two shoulders are not shown here in the image, and that the whole tooth is about 45um in length. As the tooth gets further away

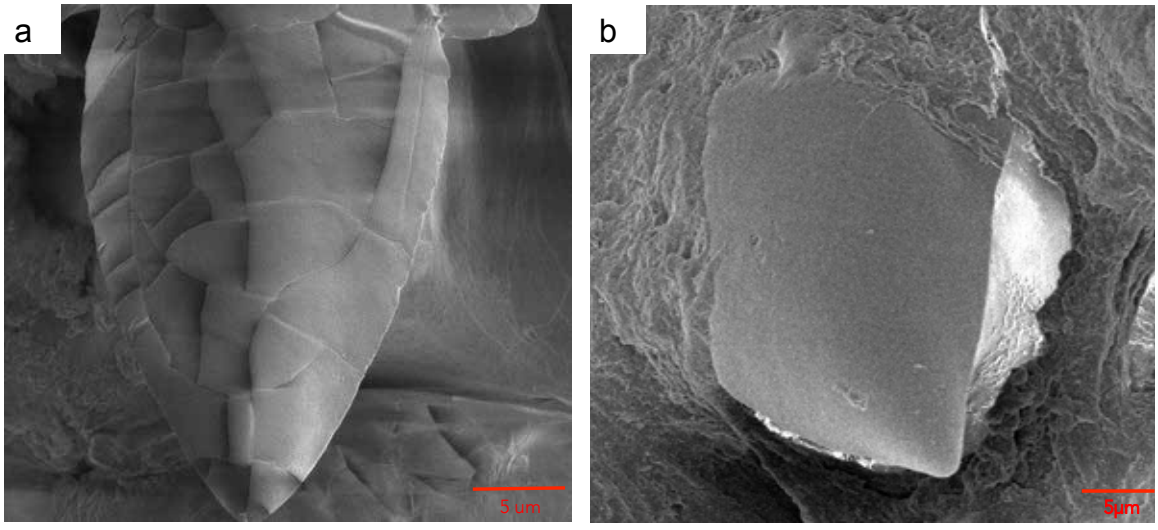

Figure 4.4.2 SEM images of banana slug radula teeth at different regions of the radula, (a) a medial tooth at the upper center area (closer to jaw), (b) a lower center tooth (farthest from jaw). Scale bars are 5um.

from the jaw, its size decreases significantly, to about 20um in length as seen in Fig. 4.4.2b.

Further investigation on the elemental composition of such plate-like structure is carried out using Energy Dispersive X-ray Spectroscopy (EDS). (Fig. 4.4.3) Preliminary data shows the presence of calcium-rich minerals with trace amount of sodium, magnesium, phosphate and sulfur. (Fig.4.4.3b, c) It is important to notice that there is a slight arbitrary

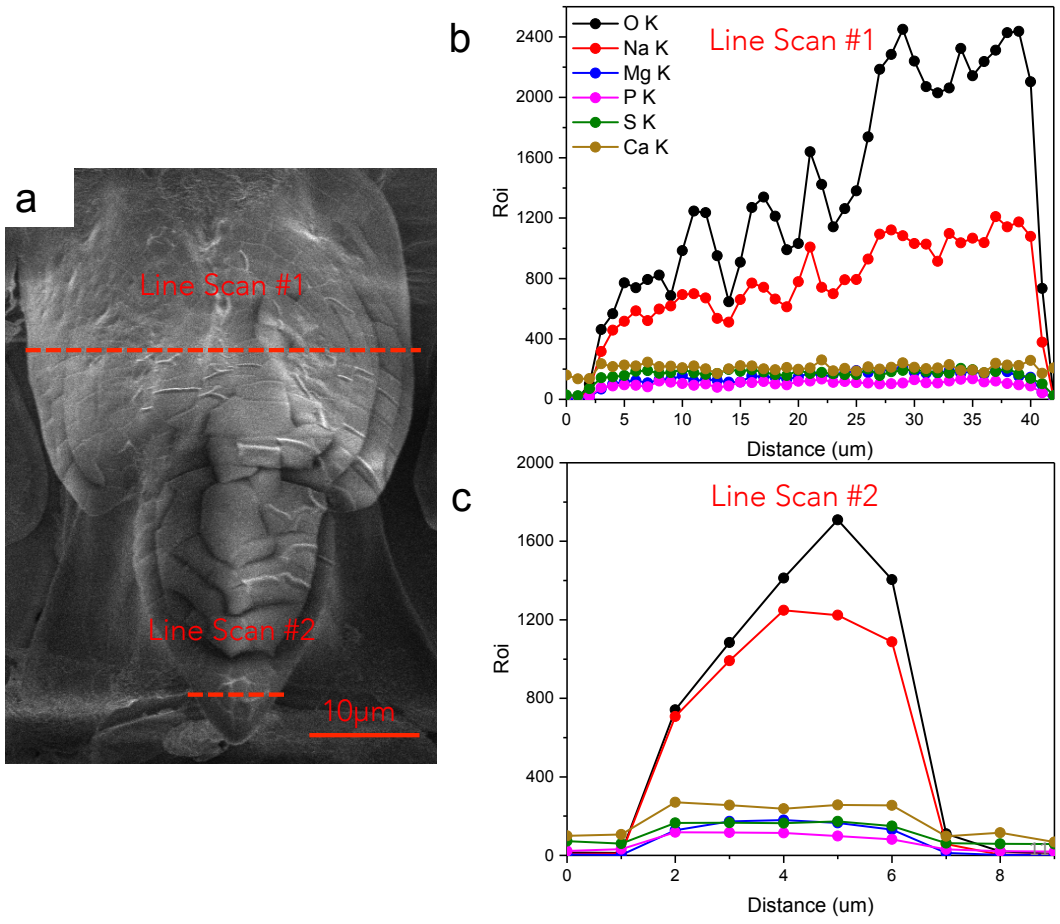

Figure. 4.4.3 (a) SEM image of a banana slug radula medial tooth that is at the upper center area, which EDS line scans are conducted. (b,c) EDS line scan results.

count increase from the inner part of the tooth (Line Scan #1) to the tip of the tooth (Line Scan #2), which may serve as an indicator that the tip of the tooth is more highly mineralized as compared to the other parts. Such a trend has been previously confirmed with the tooth of chiton,[117] but further quantitative analysis on banana slug radula teeth needs to be carried out to confirm such hypothesis. Nevertheless, there is a 5:3 counts correlation by calculating the count ratio between Calcium and Phosphate, which indicates the mineral is an apatite-rich material. Knowing that chiton needs to chew rocks, which requires ultra-high hardness from magnetite,[30] it is expected that for banana slug radula, the natural habitat of which is abundant with leafs and grass, there is no need for high hardness. Thus the mineral within banana slug radula teeth is apatite instead. This finding serves as an inspiration for efficient biological function designs.

4.5. Conclusions

All together, we have confirmed that each tooth is a natural nanocomposite that is mainly composed of an organic chitin matrix with trace amounts of calcium-rich minerals. Further EDS studies needs to be conducted on the smaller lower back tooth to confirm the hypothesis that those teeth are less or not mineralized, and are the younger teeth. Mechanical testing for teeth in different regions also needs to be investigated and to help understand the position-functionality relationship. These findings serve as a first-of-its-kind detailed characterization of terrestrial mollusk radula teeth, and provide insights on correlations from teeth morphology, chemical composition and structural hierarchy, to mechanical behavior and feeding functions, which later can be integrate into designing chitin-silk- mineral

composite for enhanced mechanical performance as the mineralized biomimetics.

Chapter V Future Outlook

In order to create the natural biomimetic hierarchy, many aspects for materials synthesis and processing must be understood. In particular, the following several issues need to be tackled at present, and will largely help the development of this area.

One is the solubility issue of chitin. As it is described in early chapters, conventional strong acid with mechanical disintegration results in chitin nanofibers magnitudes larger than their natural counterpart. HFIP method developed in The Rolandi Group successfully induces the chitin nanofiber self-assembly with 3nm in diameter. However, in order for chitin to be widely utilized in industry, water processing is more desirable. Ionic Liquid method may be a viable way to solve this problem, although chitin nanofiber self-assembly from ionic liquid is not achieved so far. Thus, developing a water-processable method that could induce chitin nanofiber self-assembly is still a pressing issue.

The second aspect is with regard to the chitin-silk-like protein assembly. As we recall the hierarchy structure as it is in the crustacean shells, chitin nanofibers are uniformly wrapped with proteins. Similarly as it is in squid beaks, a chitin nanofiber network wraps with proteins, and proteins further cross-link to reinforce the structure. So far, work has demonstrated that chitin from HFIP solution self-

assembles within either silk or GelMA matrix. However, there is a lack of structural control at the nanoscale. One question remains is that whether the protein wraps chitin fibers uniformly. Localized elastic modulus mapping with the aid of AFM might be a solution to visualize the chitin/protein distribution within the matrix, although processing methods still need to be improved in order to achieve a uniform and fully controlled network. Moreover, the electric-field assisted gelation method could potentially become a first-of-its-kind technique for aligning chitin nanofibers as a proof-of-concept but the experimental set-up needs to be scaled down. According to what has been reported in literature, in order to utilize dieletrophoretic forces to drive chitin molecules, the distance between two electrodes needs to be below 10um while using a lab-safe DC voltage below 10V. Building on the potential fiber alignment, further studies on how a Bouligand structure could reinforce materials will be an important step to truly enhance the elastic modulus, tensile strength and the toughness of such chitin-protein materials.

Lastly with regard the mineralization of materials, so far I have demonstrated the elemental difference in banana slug radula teeth where the tip is more calcium-rich compared to the inner region of the tooth. This is an interesting finding in terms of materials design. One key advantage for chitin-based structural material is its lightweight. Thus how to design a material with the most efficient mineralization with enhanced mechanical stiffness and strength while preserving its lightweight property becomes critical. Studies on natural mineralization serve as inspirations

for these biomimetic designs. Quantitative studies as well as nano-mechanical studies shall be carried out to better understand this model, building on which, a synthetic lightweight, locally mineralized composite with outstanding hardness can be achieved.

BIBLIOGRAPHY

1. M. Rinaudo, *Prog. Polym. Sci.*, 2006, **31**, 603-632.
2. J. F. V. Vincent and U. G. K. Wegst, *Arthropod Struct. Dev.*, 2004, **33**, 187-199.
3. J. F. V. Vincent, *Composites Part A*, 2002, **33**, 1311-1315.
4. P. Y. Chen, A. Y. M. Lin, J. McKittrick and M. A. Meyers, *Acta biomaterialia*, 2008, **4**, 587-596.
5. G. Falini, S. Albeck, S. Weiner and L. Addadi, *Science*, 1996.
6. C. K. S. Pillai, W. Paul and C. P. Sharma, *Prog. Polym. Sci.*, 2009, **34**, 641-678.
7. E. Khor, *Chitin: Fulfilling a Biomaterials Promise*, Elsevier Science Limited, 2001, illustrated edn., 2001.
8. M. Rolandi and R. Rolandi, *Adv Colloid Interface Sci*, 2014, **207**, 216-222.
9. E. Atkins, *J. Biosci.*, 1985, **8**, 375-387.
10. A. Miserez, T. Schneberk, C. Sun, F. W. Zok and J. H. Waite, *Science*, 2008, **319**, 1816-1819.
11. A. Miserez, Y. Li, J. H. Waite and F. Zok, *Acta biomaterialia*, 2007, **3**, 139-149.
12. H. J. Waite, *J. Mar. Biol. Assoc. U. K.*, 1985, **65**, 359-371.
13. M. Sugumaran, *Adv Insect Physiol*, 1988, **21**.
14. M. Yago, *Insect Biochem.* , 1989, **19**, 673-678.
15. T. L. Hopkins and K. J. Kramer, *Annu. Rev. Entomol.*, 1992, **37**, 273-302.
16. S. O. Andersen, M. G. Peter and P. Roepstorff, *Comp. Biochem. Physiol., Part B: Biochem. Mol. Biol.*, 1996, **113**, 689-705.
17. K. J. Kramer, M. R. Kanost, T. L. Hopkins, H. Jiang, Y. Zhu, R. Xu, J. L. Kerwin and F. Turecek, *Tetrahedron*, 2001, **57**.
18. M. E. Lynge, R. van der Westen, A. Postma and B. Städler, *Nanoscale*, 2011, **3**, 4916-4928.
19. D. R. Dreyer, D. J. Miller, B. D. Freeman, D. R. Paul and C. W. Bielawski, *Langmuir*, 2012, **28**, 6428-6435.
20. F. Bernsmann, V. Ball, F. Addiego, A. Ponche, M. Michel, J. J. Gracio, V. Toniazzo and D. Ruch, *Langmuir*, 2011, **27**, 2819-2825.
21. S. Hong, Y. Na, S. Choi, I. Song, W. Kim and H. Lee, *Adv. Funct. Mater.*, 2012, **22**, 4711-4717.
22. L. Q. Wu, M. K. McDermott, C. Zhu, R. Ghodssi and G. F. Payne, *Adv. Funct. Mater.*, 2006, **16**, 1967-1974.
23. N. F. Vecchia, R. Avolio, M. Alfè, M. E. Errico, A. Napolitano and M. d'Ischia, *Adv. Funct. Mater.*, 2013, **23**, 1331-1340.
24. S. Weiner and L. Addadi, *J. Mater. Chem.*, 1997, **7**, 689.
25. D. Raabe, C. Sachs and P. Romano, *Acta Mater.*, 2005, **53**, 4281-4292.
26. J. Y. Sun and B. Bhushan, *Rsc Adv*, 2012, **2**, 7617-7632.
27. R. A. A. M. a. C. Muzzarelli, ed., *Chitin nanofibrils. In: Chitin and Chitosan, Opportunities and Challenges*, New Age International, New Delhi, India, 2005.
28. A. Morin and A. Dufresne, *Macromolecules*, 2002, **35**, 2190-2199.
29. H. Lowenstam, *Bull. Geol. Soc. Am.*, 1962, 435-438.
30. L. M. Gordon and D. Joester, *Nature*, 2011, **469**, 194-197.
31. H. K. No, S. P. Meyers and K. S. Lee, *J. Agric. Food Chem*, 1989, **37**, 575-579.

32. A. Percot, C. Viton and A. Domard, *Biomacromolecules*, 2003, **4**, 12-18.
33. J. Li, J. F. Revol and R. H. Marchessault, *J. Appl. Polym. Sci.*, 1997, **65**, 373-380.
34. J. F. Revol and R. H. Marchessault, *Int. J. Biol. Macromol*, 1993, **15**, 329-335.
35. K. Gopalan Nair and A. Dufresne, *Biomacromolecules*, 2003, **4**, 657-665.
36. Y. Lu, L. Weng and L. Zhang, *Biomacromolecules*, 2004, **5**, 1046-1051.
37. S. Ifuku, M. Nogi, K. Abe, M. Yoshioka, M. Morimoto, H. Saimoto and H. Yano, *Biomacromolecules*, 2009, **10**, 1584-1588.
38. S. Ifuku, M. Nogi, M. Yoshioka, M. Morimoto, H. Yano and H. Saimoto, *Carbohydr. Polym.*, 2010, **81**, 134-139.
39. J. D. Goodrich and W. T. Winter, *Biomacromolecules*, 2007, **8**, 252-257.
40. S. Ifuku, M. Nogi, K. Abe, M. Yoshioka and M. Morimoto, *Carbohydr. Polym.*, 2011, **84**, 762-764.
41. M. Paillet and A. Dufresne, *Macromolecules*, 2001, **34**, 6527-6530.
42. S. Ifuku, R. Nomura, M. Morimoto and H. Saimoto, *Materials*, 2011, **4**, 1417-1425.
43. J. Wu, K. Zhang, N. Girouard and J. C. Meredith, *Biomacromolecules*, 2014, **15**, 4614-4620.
44. Y. Kato, J. Kaminaga, R. Matsuo and A. Isogai, *Carbohydr. Polym.*, 2004, **58**, 421-426.
45. R. A. A. Muzzarelli, C. Muzzarelli, A. Cosani and M. Terbojevich, *Carbohydr. Polym.*, 1999, **39**, 361-367.
46. Y. Fan, T. Saito and A. Isogai, *Biomacromolecules*, 2008, **9**, 192-198.
47. C. Zhong, A. Cooper, A. Kapetanovic, Z. H. Fang, M. Q. Zhang and M. Rolandi, *Soft Matter*, 2010, **6**, 5298-5301.
48. Y. Zhang, J. Jiang and L. Liu, *Nanoscale Res. Lett.*, 2015, **10**, 226.
49. D. X. Oh, Y. Cha, H.-L. Nguyen, H. Je, Y. Jho, D. Hwang and D. Yoon, *Sci. Rep.*, 2016, **6**, 23245.
50. H. Tamura, H. Nagahama and S. Tokura, *Cellulose*, 2006, **13**, 357-364.
51. R. Jayakumar, M. Prabaharan, S. V. Nair and H. Tamura, *Biotechnol Adv*, 2010, **28**, 142-150.
52. B.-M. Min, S. W. Lee, J. N. Lim, Y. You, T. S. Lee, P. H. Kang and W. H. Park, *Polymer*, 2004, **45**, 7137-7142.
53. H. K. Noh, S. W. Lee, J.-M. Kim, J.-E. Oh, K.-H. Kim, C.-P. Chung, S.-C. Choi, W. H. Park and B.-M. Min, *Biomaterials*, 2006, **27**, 3934-3944.
54. H. Xie, S. Zhang and S. Li, *Green Chem.*, 2006, **8**, 630.
55. S. Yamazaki, A. Takegawa, Y. Kaneko, J.-i. Kadokawa, M. Yamagata and M. Ishikawa, *Electrochem. Commun.*, 2009, **11**, 68-70.
56. Y. Wu, T. Sasaki, S. Irie and K. Sakurai, *Polymer*, 2008, **49**, 2321-2327.
57. N. Sun, R. P. Swatloski, M. L. Maxim, M. Rahman, A. G. Harland, A. Haque, S. K. Spear, D. T. Daly and R. D. Rogers, *J. Mater. Chem.*, 2008, **18**, 283-290.
58. Y. Qin, X. Lu, N. Sun and R. D. Rogers, *Green Chem.*, 2010, **12**, 968.
59. Y. Huang, Z. Zhong, B. Duan, L. Zhang and Z. Yang, *J. Mater. Chem. B*, 2014, **2**, 3427-3432
60. C. Zhong, A. Kapetanovic, Y. Deng and M. Rolandi, *Adv Mater*, 2011, **23**, 4776-4781.

61. P. Hassanzadeh, W. Sun, J. P. de Silva, J. Jin, K. Makhnejia, G. L. W. Cross and M. Rolandi, *J. Mater. Chem. B*, 2014, **2**, 2461-2466.
62. R. M. N. V. Kumar, R. A. A. Muzzarelli, C. Muzzarelli, H. Sashiwa and A. J. Domb, *Chemical Reviews*, 2004, **104**, 6017-6084.
63. J. Berger, M. Reist, J. M. Mayer, O. Felt and N. A. Peppas, *Eur. J. Pharm. Biopharm.*, 2004, **57**, 19-34.
64. N. Bhattarai, J. Gunn and M. Zhang, *Chitosan-based hydrogels for controlled, localized drug delivery*, 2010, **62**, 83-99.
65. K. Ono, Y. Saito, H. Yura and K. Ishikawa, *J. Biomed. Mater. Res.*, 2000, **49**, 289-295.
66. J. Z. Knaul and K. A. M. Creber, *J. Appl. Polym. Sci.*, 1997, **66**, 117-127.
67. G. C. East and Y. Qin, *Journal of applied polymer science*, 1993, **50**, 1773-1779.
68. H. Tamura, Y. Tsuruta and K. Itoyama, *Carbohydr. Polym.*, 2004, **56**, 205-211.
69. L. Notin, C. Viton, J.-M. Lucas and A. Domard, *Acta biomaterialia*, 2006, **2**, 297-311.
70. B. Duan, L. Wu, X. Li, X. Yuan, X. Li, Y. Zhang and K. Yao, *Journal of Biomaterials Science, Polymer Edition*, 2007, **18**, 95-115.
71. N. F. Della Vecchia, R. Avolio, M. Alfè, M. E. Errico, A. Napolitano and M. d'Ischia, *Adv. Funct. Mater.*, 2013, **23**, 1331-1340.
72. Y. Tan, S. Hoon, P. A. Guerette, W. Wei, A. Ghadban, C. Hao, A. Miserez and J. H. Waite, *Nat. Chem. Biol.*, 2015, **11**, 488-495.
73. N. E. Suyatma, L. Tighzert, A. Copinet and V. Coma, *J. Agric. Food Chem.*, 2005, **53**, 3950-3957.
74. M. Zhang, X. H. Li, Y. D. Gong, N. M. Zhao and X. F. Zhang, *Biomaterials*, 2002, **23**, 2641-2648.
75. X. O. Dongyeop and H. Dong, *Biotechnol. Prog.*, 2013, **29**, 505-512.
76. J. D. Schiffman and C. L. Schauer, *Biomacromolecules*, 2007, **8**, 594-601.
77. P. L. Bruce, L. D. Jeffrey and B. M. Phillip, *Biomacromolecules*, 2002, **3**, 1038-1047.
78. J. G. Fernandez and D. E. Ingber, *Adv. Mater.*, 2012, **24**, 480-484.
79. L. Shao, G. Kumar, J. L. Lenhart, P. J. Smith and G. F. Payne, *Enzyme Microb. Technol.*, 1999, **25**, 660-668.
80. L. Q. Wu, H. D. Embree and B. M. Balgley, *Environ. Sci. Technol.*, 2002, **36**, 3446-3454.
81. Y. Liu, K. Ai and L. Lu, *Chem. Rev.*, 2014, **114**, 5057-5115.
82. S. O. Andersen, *Insect Biochem. Mol. Biol.*, 2010, **40**, 166-178.
83. L. Q. Wu, R. Ghodssi, Y. A. Elabd and G. F. Payne, *Adv. Funct. Mater.*, 2005, **15**, 189-195.
84. L. Q. Wu, M. K. McDermott, C. Zhu, R. Ghodssi and G. F. Payne, *Adv. Funct. Mater.*, 2006, **16**, 1967-1974.
85. K. M. Gray, E. Kim, L.-Q. Wu, Y. Liu, W. E. Bentley and G. F. Payne, *Soft Matter*, 2011, **7**, 9601-9615.
86. J. H. Ryu, S. Jo, M. Y. Koh and H. Lee, *Adv. Funct. Mater.*, 2014, **24**, 709-7716.
87. B. P. Lee, J. L. Dalsin and P. B. Messersmith, *Biomacromolecules*, 2002, **3**, 1038-1047.

88. X. Du, L. Li, J. Li, C. Yang, N. Frenkel, A. Welle, S. Heissler, A. Nefedov, M. Grunze and P. A. Levkin, *Adv. Mater.*, 2014, **26**, 8029-8033.
89. I. M. Vold and B. E. Christensen, *Carbohydrate research*, 2005, **340**, 679-684.
90. D. N. Moses, M. A. Mattoni, N. L. Slack, J. H. Waite and F. W. Zok, *Acta biomaterialia*, 2006, **2**, 521-530.
91. U. G. K. Wegst and M. F. Ashby, *Philos. Mag.*, 2004, **84**, 2167-2181.
92. R.N. Carson and J. T. Staley, in *ASM Handbook*, ed. G. E. Dieter, ASM International, 1997, vol. 20, pp. 383-415.
93. B. E. Christensen, I. M. N. Vold and K. M. Vårum, *Carbohydr. Polym.*, 2008, **74**, 559-565.
94. Y. Shigemasa, H. Matsuura, H. Sashiwa and H. Saimoto, *Int. J. Biol. Macromol.*, 1996, **18**, 237-242.
95. M. D. Frogley, D. Ravich and D. H. Wagner, *Compos. Sci. Technol.*, 2003, **63**, 1647-1654.
96. J. D. Fox, J. R. Capadona, P. D. Marasco and S. J. Rowan, *Journal of the American Chemical Society*, 2013, **135**, 5167-5174.
97. D. Ding, P. A. Guerette, J. Fu, L. Zhang, S. A. Irvine and A. Miserez, *Adv. Mater.*, 2015, **27**, 3953-3961.
98. J. Jin, P. Hassanzadeh, G. Perotto, W. Sun, M. A. Brenckle, D. Kaplan, F. G. Omenetto and M. Rolandi, *Adv Mater*, 2013, **25**, 4482-4487.
99. M. Lescanne, A. Colin, O. Mondain-Monval and K. Heuzé, *Langmuir*, 2002, **18**, 7151-7153.
100. M. I. Boamfa, P. C. M. Christianen and H. Engelkamp, *Adv. Funct. Mater.*, 2004.
101. L. Sardone, V. Palermo and E. Devaux, *Adv. Mater.*, 2006, **18**, 1276-1280.
102. B. W. Messmore, J. F. Hulvat and E. D. Sone, *Journal of the American Chemical Society*, 2004, **126**, 14452-14458.
103. A. Bezryadin, C. Dekker and G. Schmid, *Appl. Phys. Lett.*, 1997, **71**, 1273-1275.
104. X. Duan, Y. Huang, Y. Cui, J. Wang and C. M. Lieber, *Nature*, 2001, **409**, 66-69.
105. M. D. Lynch and D. L. Patrick, *Nano Lett.*, 2002, **2**, 1197-1201.
106. G. Maubach and W. Fritzsche, *Nano Lett.*, 2004, **4**, 607-611.
107. B. V. Ban E, Shephard MS, Picu CR, *J Appl Mech*, 2016, **83**, 410081-410087.
108. M. J. Buehler, *Proceedings of the National Academy of Sciences*, 2006, **103**, 12285-12290.
109. X. Hu, K. Shmelev, L. Sun, E.-S. S. Gil, S.-H. H. Park, P. Cebe and D. L. Kaplan, *Biomacromolecules*, 2011, **12**, 1686-1696.
110. H. J. Jin and D. L. Kaplan, *Nature*, 2003, **424**, 1057-1061.
111. Z. S. Galis and J. J. Khatri, *Circ. Res.*, 2002.
112. D. E. Discher, P. Janmey and Y. Wang, *Science*, 2005, **310**, 1139-1143.
113. P. Hassanzadeh, M. Kharaziha, M. Nikkhah, S. R. Shin, J. Jin, S. He, W. Sun, C. Zhong, M. R. Dokmeci, A. Khademhosseini and M. Rolandi, *J Mater Chem B Mater Biol Med*, 2013, **1**.
114. N. Annabi, S. M. Mithieux, P. Zorlutuna, G. Camci-Unal, A. S. Weiss and A. Khademhosseini, *Biomaterials*, 2013, **34**, 5496-5505.
115. H. K. Kleinman and G. R. Martin, *Semin Cancer Biol*, 2005, **15**, 378-386.
116. C. Helary, I. Bataille, A. Abed, C. Illoul, A. Anglo, L. Louedec, D. Letourneur, A. Meddahi-Pelle and M. M. Giraud-Guille, *Biomaterials*, 2010, **31**, 481-490.

117. Q. Wang, M. Nemoto, D. Li, J. C. Weaver, B. Weden, J. Stegemeier, K. N. Bozhilov, L. R. Wood, G. W. Milliron, C. S. Kim, E. DiMasi and D. Kisailus, *Adv. Funct. Mater.*, 2013, **23**, 2908-2917.
118. C. D. Rollo, *Researches on Population Ecology*, 1983, **25**, 20-43.
119. A. B. Harper, *The Banana Slug*, Bay Leaves Press, Aptos, California, 1988.
120. K. O. Richter, *The Veliger*, 1980, **23**, 43-47.
121. H. E. Quick, *British slugs (Pulmonata: Testacellidae.*, Arionidae, Lima, 1960.
122. R. Moens, and A. Rassel, *Annales de la Societe Royale Zoologique de Belgique* 1985.
123. N. W. Runham, and P. R. Thornton, *J. Zool.*, 1967, **153**, 445-452.
124. K. Kerth, *Cell Tissue Res.*, 1979, **203**, 283-289.